

Olea, Maria ORCID: https://orcid.org/0000-0002-1854-8950 and Sasaki, Takehiko (2025) Active and coking resistant Ni/SBA-15 catalysts for low temperature dry reforming of methane. Processes, 13 (11). p. 3505.

Downloaded from: https://insight.cumbria.ac.uk/id/eprint/9181/

University of Cumbria will soon be migrating from Insight (the current EPrints repository) to Pure research information system. Existing research outputs currently in Insight will be migrated to Pure. For now, no action is required from researchers. Training and support will be available to help in the transition to the new platform.

Usage of any items from the University of Cumbria's institutional repository 'Insight' must conform to the following fair usage quidelines.

Any item and its associated metadata held in the University of Cumbria's institutional repository Insight (unless stated otherwise on the metadata record) may be copied, displayed or performed, and stored in line with the JISC fair dealing guidelines (available here) for educational and not-for-profit activities

provided that

- the authors, title and full bibliographic details of the item are cited clearly when any part of the work is referred to verbally or in the written form
 - a hyperlink/URL to the original Insight record of that item is included in any citations of the work
- the content is not changed in any way
- all files required for usage of the item are kept together with the main item file.

You may not

- sell any part of an item
- refer to any part of an item without citation
- amend any item or contextualise it in a way that will impugn the creator's reputation
- remove or alter the copyright statement on an item.

The full policy can be found here.

Alternatively contact the University of Cumbria Repository Editor by emailing insight@cumbria.ac.uk.





Article

Active and Coking Resistant Ni/SBA-15 Catalysts for Low Temperature Dry Reforming of Methane †

Maria Olea 1,* o and Takehiko Sasaki 2

- School of Computing, Engineering & Digital Technologies, Teesside University, Southfield Rd, Tees Valley, Middlesbrough TS1 3BX, UK
- Graduate School of Frontier Sciences, The University of Tokyo, Kashiwa 277-8561, Japan; tksasaki@edu.k.u-tokyo.ac.jp
- * Correspondence: m.olea@tees.ac.uk
- [†] In memory of Professor John Gleaves—inventor of TAP Reactor.

Abstract

In recent years CO₂ reforming of methane has attracted great interest as it produces high CO/H₂ ratio syngas suitable for the synthesis of higher hydrocarbons and oxygenated derivatives since it is a way for disposing and recycling two greenhouse gases with high environmental impact, CH₄ and CO₂, and because it is regarded as a potential route to store and transmit energy due to its strong endothermic effect. Along with noble metals, all the group VIII metals except for osmium have been studied for catalytic CO₂ reforming of methane. It was found that the catalytic activity of Ni, though lower than those of Ru and Rh, was higher than the catalytic activities of Pt and Pd. Although noble metals have been proven to be insensitive to coke, the high cost and restricted availability limit their use in this process. It is therefore valuable to develop stable Ni-based catalysts. In this contribution, we show how their activity and coking resistivity are greatly related to the size and dispersion of Ni particles. Well-dispersed Ni nanoparticles were achieved by multistep impregnation on a mesoporous silica support, namely SBA-15, obtained through a sol-gel method, using acetate as a nickel precursor and keeping the Ni loading between 5% and 11%. Significant catalytic activity was obtained at temperatures as low as 450 °C, a temperature well below their deactivation temperature, i.e., 700 °C. For the pre-reduced samples, a CO₂ conversion higher than 99% was obtained at approximately 680 °C. As such, their deactivation by sintering and coke formation was prevented. To the best of our knowledge, no Ni-based catalysts with complete CO2 conversion at temperatures lower than 800 °C have been reported so far.

Keywords: dry reforming of methane; Ni/SBA-15 catalysts; TAP reactor



Academic Editor: Mariana de Mattos V. M. Souza

Received: 26 September 2025 Revised: 20 October 2025 Accepted: 25 October 2025 Published: 31 October 2025

Citation: Olea, M.; Sasaki, T. Active and Coking Resistant Ni/SBA-15 Catalysts for Low Temperature Dry Reforming of Methane. *Processes* **2025**, 13, 3505. https://doi.org/10.3390/ pr13113505

Copyright: © 2025 by the authors. Licensee MDPI, Basel, Switzerland. This article is an open access article distributed under the terms and conditions of the Creative Commons Attribution (CC BY) license (https://creativecommons.org/licenses/by/4.0/).

1. Introduction

Recent global energy deficiency and more severe emission regulations, especially for CO₂, have motivated worldwide research on the valorisation of biomass as a source of renewable energy and fuels. Seen as a way to mitigate global warming and diversify the energy sources, the use of biomass for fuels, power production, and chemicals that would otherwise be made from fossil fuels provides many benefits. Beside direct combustion, the fermentation of carbohydrates to ethanol or first generation biofuels, the fermentation of lignocellulosic feedstock to second generation biofuels, the cultivation of oil seeds for biodiesel, and the generation of biogas via anaerobic digestion followed by a further catalytic conversion of biogas to syngas or "green gas" through dry reforming and then

Processes 2025, 13, 3505 2 of 22

by a Fischer–Tropsch (FT) transformation to synoil were considered. Our work focuses on using advanced catalysis to develop sustainable technologies for chemicals, fuels, and energy, with the ultimate goal of zero waste and zero pollution.

Lately, there have been considerable efforts to develop cost-effective processes for converting natural gas, composed mainly of methane, to fuels, fuel additives, and chemicals. One potential route involves the conversion of methane via a dry reforming of methane (DRM) process to a syngas intermediate suitable for the synthesis of desired products using Fischer–Tropsch technology; however, the viability of these processes has been hampered by both cost and technical limitations. One potential option to reduce the cost of syngas production (which typically represents more than 60% of the process cost) is the utilization of renewable resources such as biogas. As biogas consists mainly of CH₄ and CO₂, the most suitable process for its utilization is the dry reforming of methane (DRM) to syngas and then to liquid energy carriers via Fischer-Tropsch technology. The DRM process provides both a way for disposing of and recycling CO₂ and CH₄, two greenhouse gases with high environmental impact [1], using an alternative route for producing syngas with higher purity and lower H₂/CO ratio than steam reforming and partial oxidation [2]. Lower H₂/CO ratio syngas is ideal for the Fischer–Tropsch synthesis of long-chain hydrocarbons, while higher purity syngas is a preferable feedstock for hydrogen production. Hydrogen is emerging as a future replacement fuel for traditional fossil fuels, possibly ensuring energy security and environmental viability [3]. Although the DRM process has many environmental and economic incentives, unfortunately, at the present time, there are no commercial processes for the reforming of methane with CO₂.

This study seeks to explore a potential new catalytic approach that might be developed to achieve this.

Key to the efficient production of syngas by DRM is the use of an effective catalyst. Presently, noble metal catalysts, such as Rh [4], Ru, and Pt [5–7], are used in such processes as they exhibit outstanding catalytic activity. However, noble metal catalysts suffer from several disadvantages, including high cost and poor availability. Further research has shown that transition metal catalysts, such as nickel, may offer a suitable alternative as they are low cost, easily accessible, and offer high activity and selectivity toward the production of syngas from DRM [8–16]. Despite their apparent suitability, nickel catalysts are easily deactivated at temperatures higher than 700 °C. Deactivation occurs through two mechanisms, one known as sintering, which involves an increase in metal crystallite growth leading to the loss of exposed metal surface area and changes in the catalytic properties, and another known as coking, which involves carbon and coke-forming processes [17,18]. Nickel catalyses carbon formation via hydrocarbon decomposition and CO disproportionation reactions. To date, only one pilot plant scale-up has been attempted, and although high conversion rates of carbon dioxide were achieved, the process was considered commercially unattractive as the operating temperature (namely 800 °C) was over their deactivation temperature [19]. Therefore, the challenge is to develop highly active catalysts that exhibit a high selectivity toward hydrogen and carbon monoxide without forming carbon.

It has been reported that highly dispersed Ni catalysts show good coke resistance [20,21], while the use of supports such as titania, alumina, or silica offers high thermal stability [11,22]. However, despite all the research efforts, supported Ni catalysts that are highly active at temperatures lower than their deactivation temperature, and as such, suitable for commercial applications, have not been reported yet.

A suggested solution to inhibit the carbon deposition has been to promote the Nibased catalysts with a metal oxide, especially CeO₂ (which, due to its redox properties, would induce the formation of oxygen vacancies, responsible for enhanced mobility of surface oxygen, which, in turn, would contribute to lowering the carbon deposition on the Processes 2025, 13, 3505 3 of 22

metallic particles), or with ceria-zirconia mixed oxides [23]. Nevertheless, good activity was observed, but by adding an extra element (or two), the cost of the Ni/SBA-15 catalysts will increase, and as such, higher prices will hamper their commercialization.

What is more, most of the studies on DRM reaction over Ni-based catalysts have been performed using a CH_4 : CO_2 ratio of 1:1, a ratio that would favor less carbon formation via methane decomposition. In our study, a CH_4 : CO_2 ratio of 1.5:1 is used instead, a ratio closer to the one in the biogas.

Therefore, we have recently focused our work on the preparation and characterization of nickel-based catalysts suitable for commercial applications. Their extensive physical and chemical characterization has allowed us to assess the way preparation conditions affect the structure, morphology, texture, resistance to coke formation, stability, and finally, the catalytic activity. Single- and/or multiple-step impregnation of nickel precursors, acetate, nitrate, and citrate, onto a mesoporous silica support, i.e., SBA-15, obtained through a sol-gel method, was carried out under different preparation conditions. SBA-15 was chosen as support due to a relatively well-defined geometry, involving ordered hexagonal arrays of mesopores, with a tunable pore size and high surface area. Samples with increasing Ni loading from 1 wt% to 30 wt% were prepared by single-step impregnation of nickel nitrate. Both single- and multiple-step impregnation methods of nickel acetate were used to prepare samples with Ni loading from 1 wt% to 11 wt%. When nickel citrate was used as a precursor, the maximum Ni loading was 15 wt% for the single-step impregnation. The knowledge gained through this very demanding preparation process allowed us to identify the conditions to be used to synthesize optimal formulation catalysts, allowing us to better understand the structure-activity relationship of these Ni-based catalysts. We have found that the best dispersion of nickel species over the mesoporous support was achieved by using acetate as the nickel precursor, while a nickel loading between 5% and 11% obtained through the multiple-step impregnation was responsible for the highest activity and resistance to coke formation of these catalysts.

Hence, in light of the above considerations, this paper presents the synthesis and characterization of two samples, the 5 wt% and 11 wt% Ni ones, as catalysts, with Ni loadings within this window that are the most likely to be used for commercial applications. What is more, by using a $CH_4:CO_2$ ratio closer to the one in biogas, a sustainable DRM commercial technology can be developed further if the two catalysts prove to be active and selective and, at the same time, resistant to coke formation.

2. Materials and Methods

2.1. Synthesis of Support, SBA-15

The general experimental procedure followed in the preparation of SBA-15 meso-porous silica was described in detail by Zhao et al. [24,25]. This procedure was modified, and the preparation conditions were optimized through experiments. The optimized procedure is described below.

A total of 4 g of tri-block copolymer of poly(ethylene oxide)-poly(propylene oxide)-poly(ethylene oxide) (EO $_{20}$ PO $_{70}$ EO $_{20}$ or Pluronic P_{123} , with a typical $M_n = 5800$) was dissolved in 130 g deionized water. The formed solution was kept stirring at 40 °C until clear. Then, 20 mL HCl (37 wt%) was added, followed by the dropwise addition of 9.25 g of tetraethyl orthosilicate. The reaction mixture was stirred moderately for 24 h, followed by aging at 95 °C for another day without stirring. The white product was collected by filtration, dried, and then calcined at 550 °C for 6 h with the heating ramp of 1 °C/min. SBA-15 was then rehydrated in boiling water for 2 h. Obtained hydrated SBA-15 was dried at 130 °C for 3 h.

Processes 2025, 13, 3505 4 of 22

2.2. Synthesis of Catalysts

A total of 1.0 g of SBA-15 was impregnated with 12 mL of a water solution containing 0.153 g nickel acetate tetrahydrate (wet impregnation). After sonication for several minutes, the mixture was stirred for 1 h at room temperature. Impregnated silica was collected and dried at 100 $^{\circ}$ C in a vacuum and calcined at 550 $^{\circ}$ C for 2 h with a heating rate of 10 $^{\circ}$ C/min.

This process was repeated several times to increase the Ni content.

2.3. Support and Catalysts Characterization

X-ray diffraction (XRD) patterns of the support and catalyst samples were recorded on a Bruker D8 (25 kV, 20 mA) powder X-ray diffractometer, using Cu K α (λ = 0.15406 nm) radiation; the tube voltage was 40 kV, and the current was 20 mA. The data were collected from 0.5 to 4° (2 Θ) with a resolution step size of 0.01° or angular increment of 0.01° (low-angle XRD patterns) and from 10 to 100° (2 Θ) with a resolution step size of 0.02° (conventional wide-angle XRD patterns). Small-angle XRD provides information on the mesoporous structure, while wide-angle XRD provides information on the crystalline structure.

A Scanning Electron Microscopy (SEM) was used to monitor the morphology of the support and of the catalyst samples as well. SEM examination was performed using a Hitachi S-3400N electronic microscope. A beam of highly energetic electrons (0.1–50 keV) is focused on the sample surface. The microscope is equipped with a secondary electron detector, a backscattered electron (BSE) detector, and an X-ray energy dispersive spectroscopy (EDS or EDX). A secondary electron detector records topography of the surface under observation with high-resolution imaging on the order of 1–2 nm and at a magnification range from $10 \text{ to } 500,000 \times$.

Transmission electron microscopy (TEM) equipped with energy dispersive X-ray (EDX) characterization was performed on a JEOL JEM-1010 at an accelerating voltage of 100 kV. The samples were prepared in the following way: 0.02~g of each sample was dispersed in 3 mL of ethanol solution, and the suspension was sonicated for 30 min. A drop of the suspension was transferred to a Cu mesh grid covered with carbon film. The grid was dried in a vacuum at room temperature for 24 h.

The total surface area, the pore volume, and the pore size distribution were determined by nitrogen sorption at 77 K (on a Micromeritics ASAP2010 apparatus; prior to the analysis, the samples were evacuated at 473 K for 10 h) and mercury porosimetry (carried out on a Micromeritics Autopore IV 9510 analyzer). After degassing the samples, mercury was introduced at a pressure range from vacuum to 418 MPa. Measurements were performed using a contact angle of 140° for mercury and a pressure equilibration time of 10 s. The Washburn equation was applied to calculate the pore size distribution. The specific surface area was calculated using the Brunauer–Emmett–Teller (BET) method.

TeraHertz Spectroscopy (Reflectance and Transmission) measurements were acquired using a TPS Spectra 3000 spectrometer (TeraView Ltd., Cambridge, UK).

Temperature programmed reduction (CH₄-TPR), oxidation (O₂-TPO), and reaction (CH₄:CO₂ = 1.5:1) experiments were performed using a CATLAB system (Hiden Analytical, Warrington, UK) on fresh and in situ reduced Ni catalysts. Heating rates were 10 °C min⁻¹. In situ reduction was performed under a H₂ flow by heating to 550 °C at 10 °C min⁻¹ and holding at this temperature for 1 h.

X-ray photoelectron spectroscopy (XPS) was carried out on an Escalab 220 XL spectrometer (Vacuum Generators). The monochromatic Al K_X-ray source was used, and electron energies were measured in the constant analyzer energy mode. The pass energy was 100 eV for the survey of spectra and 40 eV for the single-element spectra. All XPS binding energies were referred to the C1s core level at 285 eV. The angle between the incident

Processes **2025**, 13, 3505 5 of 22

X-rays and the analyzer was 58° , with photoelectrons being collected perpendicularly to the sample surface. Spectra were analyzed with CasaXPS 2.3.26 software.

2.4. Evaluation of Catalytic Activity

The activity and selectivity toward the dry reforming of the methane reaction were tested using both steady-state and transient experiments. The steady-state experiments were performed using the Catlab system (Hiden Analytical, Warrington, UK), while the transient experiments were performed using a TAP (Temporal Analysis of Products) reactor, available at The University of Tokyo. The Catlab system consists of a feeding section, a reaction section, and an analysis section, i.e., a quadrupole mass spectrometer. The reaction section consists of a quartz tube reactor approximately 100 mm long with a radius of 5 mm filled with the required mass of catalyst (0.05 g if not otherwise specified) and placed within a programmable induction furnace. The catalyst bed was sandwiched between two quartz wool layers, while the dead volumes before and after the catalyst bed were filled with quartz chips to minimize potential homogeneous reactions at higher temperatures. The reaction gases entered the system from compressed cylinders via mass flow controllers and left the reactor, being sent to the vent. A small amount of the gas leaving the reactor was sent to the mass spectrometer for analysis.

The TAP reactor system, invented by Professor John Gleaves, has been described in detail elsewhere [26]. Briefly, the apparatus consists of a catalytic micro-reactor, a gas delivery system for introduction of either high-speed gas pulses or a continuous flow of gas, a high-throughput, high-vacuum system, and a computer-controlled quadrupole mass spectrometer. The micro-reactor is made from a stainless-steel tube whose diameter and length are 2 mm and 25 mm, respectively. Catalyst particles (about 0.005 g) are fixed in the reactor by a stainless-steel mesh. The reactor can be heated up to 1000 K by cartridge heaters. The two high-speed pulse valves can be operated at an interval of up to 50 pulses per second. The minimum pulse width is 200 ms. Pulse intensities were varied between 10^{13} and 10^{20} molecules per pulse. Before each experiment, the catalyst was heated at 473 K for 30 min in vacuum to desorb pre-adsorbed species. The 150 to 250 pulses in the TAP experiments were averaged to increase the signal-to-noise ratio in the response. The pulse-to-pulse reproducibility of the system was good enough for averaging.

3. Results and Discussion

3.1. Characterization Results of Support

The structure, morphology, and texture of the support and catalysts were assessed through low-angle XRD, SEM, and TEM, and physisorption measurements. Table 1 presents their physico-chemical properties.

Table 1. Physico-c	hemical propert	ies of support and	l catalysts.

Sample	d_{100} (nm)	<i>a</i> (nm)	S_{BET} (m ² /g)	Pore Diameter (nm)	Pore Vol. (cm ³ /g)
SBA-15	8.4	9.7	720	6.5	0.94
5% Ni	7.7	8.9	547	3.2	0.82
11% Ni	7.4	8.5	506	2.6	0.74

Figure 1 shows the low-angle powder XRD patterns of SBA-15. Three XRD peaks are observed at $2\theta \sim 1-4^{\circ}$, which can be indexed as (100), (110), and (200) reflections of a well-ordered 2D hexagonal (p6mm) mesostructure possessing long-range order, with a quite large unit cell [24,25], namely a = 9.7 nm (the unit cell parameter a is calculated from $a = 2d_{100}/\sqrt{3}$, where the d-spacing values are calculated by $n\lambda = 2d_{100} \sin \theta$.) The obtained

Processes 2025, 13, 3505 6 of 22

hexagonal mesostructured was expected as the volume fraction of the block copolymer, i.e., Φ_{P123} (%), in the mesostructured composite was in the range of 38–52% for H₂O-P123 and 40–55% for SiO₂-P123. Lamelar, hexagonal, or cubic mesophases can be obtained by controlling the Φ_{P123} fraction [27]. However, it should be noted that SBA-15 cannot be regarded as an ideal hexagonal lattice of pores embedded in a uniform matrix, as the structure of the silica walls is more complex. This can be easily assessed by calculating the dS/V number, where d is pore diameter, S is specific surface area, and V is pore volume. For a material possessing an ideal hexagonal geometry, this number should be equal to four [28,29]. By using the structural parameters displayed in Table 1, the value of 4.3 is obtained for the prepared SBA-5 sample, which is rather close to the theoretical value.

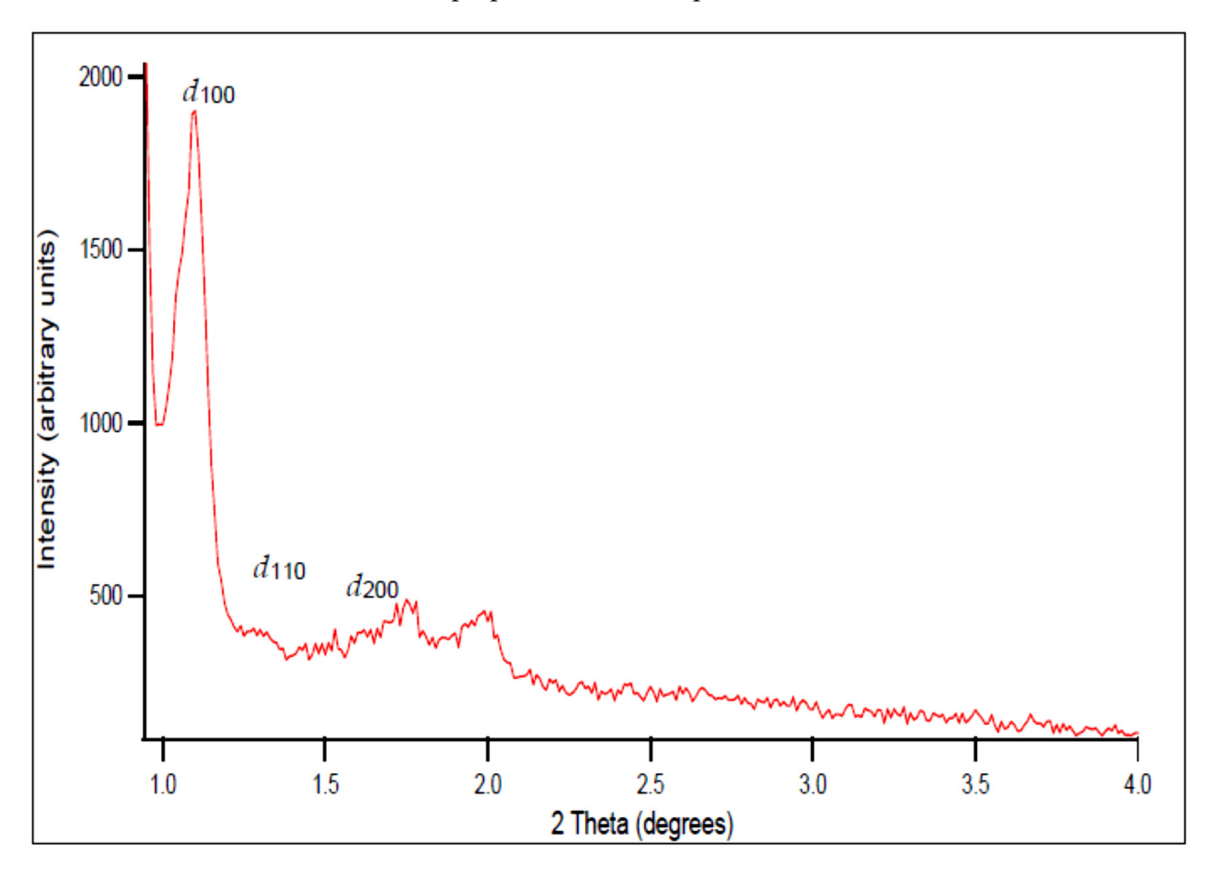


Figure 1. Low-angle XRD patterns of SBA-15, recorded using Cu K α (λ = 0.15406 nm) radiation, 40 kV tube voltage, and 20 mA current.

The SEM image reveals that the calcined SBA-15 sample consists of many fiber (rope)-like domains (Figure 2). Each fiber seems to be formed by end-to-end aggregations of apparently wheat-grain-shaped SBA-15 particles (primary particles) of 0.5–1.0 μ m in length and 0.5 μ m in width. As such, the surface energy of the hydrophilic ends due to hydroxyl groups is reduced, and their growth is encouraged in the 001 plane.

TEM measurements confirm the highly well-ordered hexagonal network of rather straight cylindrical mesopores. As seen in Figure 3, SBA-15 shows a 2D hexagonal packed array of pores with long 1D channels (p6mm plane group) [30]. The channels are interconnected by small micropores. Thus, SBA-15 exhibits mainly a mesoporous structure and possesses a small amount of micropores. The mesopore diameter was roughly estimated from TEM micrographs as between 6.3 and 6.5 nm and confirmed by the pore size distribution. The distance between mesopores (interplanar distance), d_{100} , is estimated to be ~8.5 nm, in good agreement with that determined from the XRD data, using Bragg's law.

Processes **2025**, 13, 3505 7 of 22

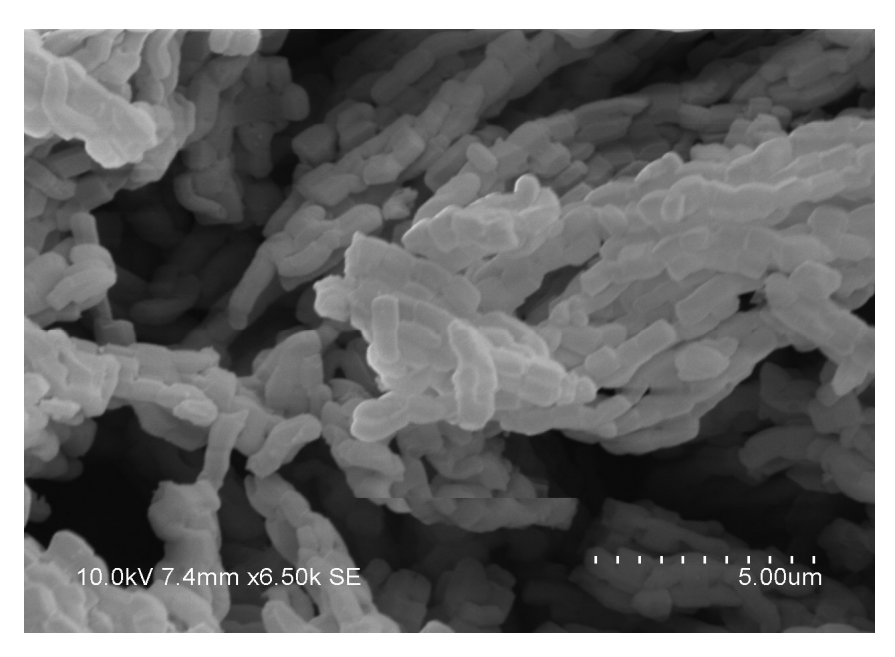
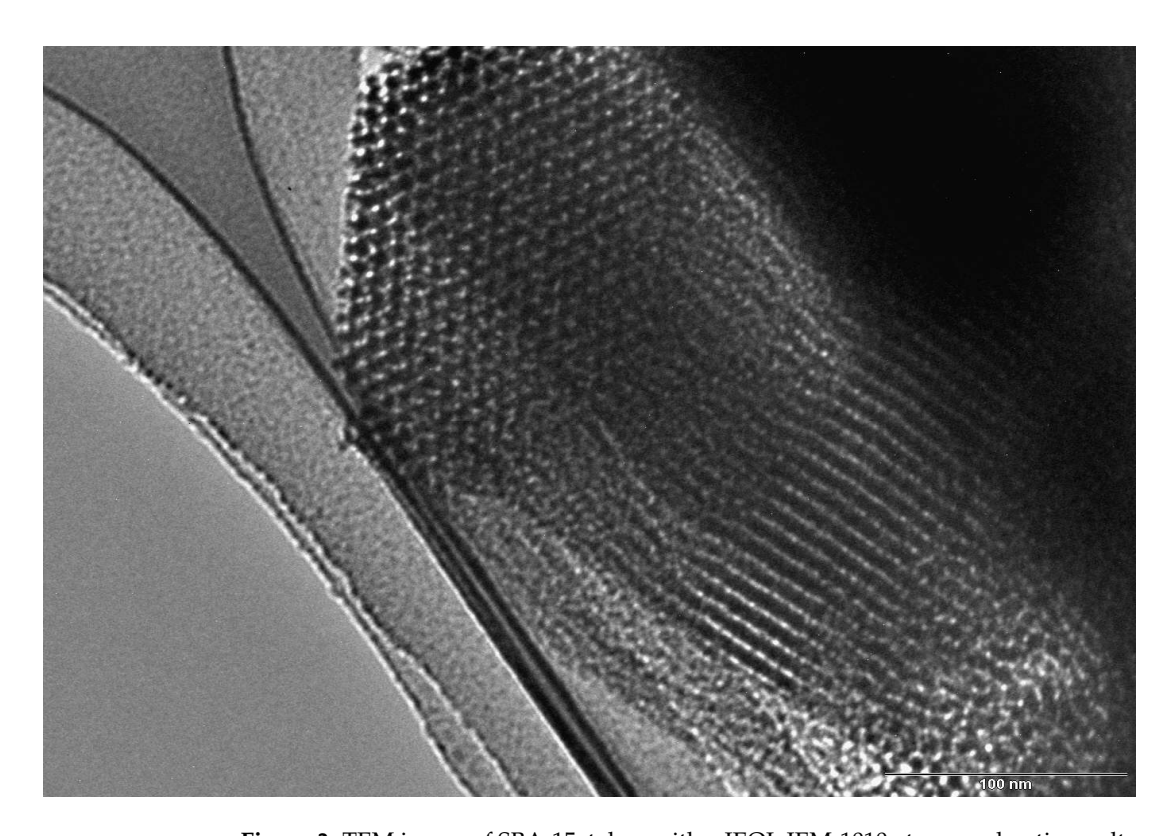


Figure 2. SEM image of SBA-15, taken with highly energetic electrons (0.1–50 keV).



 $\textbf{Figure 3.} \ \text{TEM image of SBA-15, taken with a JEOL JEM-1010 at an accelerating voltage of 100 kV.}$

The N_2 isotherms are of type IV with an H1 hysteresis loop, according to IUPAC classification, and present a steep capillary condensation step at a medium relative pressure (P/P $_0$ ~0.6), characteristic of high-quality open, nearly cylindrical large-pore SBA-15 mesoporous silica (see Figure 4). Three distinct regions can be discerned in the isotherm for the SBA-15 sample: (1) monolayer–multilayer adsorption of nitrogen on the pore walls at low pressures, (2) a sudden steep increase in the adsorbed nitrogen at intermediate pressures due to the capillary condensation, and (3) multilayer adsorption on the external surface of the particles. The broad hysteresis loop of the SBA-15 sample is caused by the presence of long mesopores connected by smaller micropores, thus hampering the filling

Processes 2025, 13, 3505 8 of 22

and emptying of the accessible volume. The sharpness of the capillary condensation steps indicates uniformity of pore channels and their narrow pore size distribution. Indeed, the pore size distribution, defined as the pore volume increment per unit logarithm of pore diameter versus the logarithm of the corresponding pore diameters, was narrow, although the SBA-15 sample shows, in addition to the main pores of 6.5 nm diameter, a pore volume of 0.94 cm 3 /g and a BET surface area of 720 m 2 /g, and the presence of smaller pores of about 3.9 nm diameters as well. The fact that there is some N_2 adsorption at very low relative pressure is evidence for the presence of micropores. Along with the N_2 adsorption measurements, mercury intrusion porosimetry measurements were performed, which evidenced the presence of intra- and inter-particles macropores, with a relatively narrow pore size distribution as well (in the range of 50–300 nm and 10–175 μ m, respectively). Figure 5A shows the cumulative specific adsorbed and intrusion volumes plotted versus the logarithm of the pore diameter, while Figure 5B presents the pore size distribution.

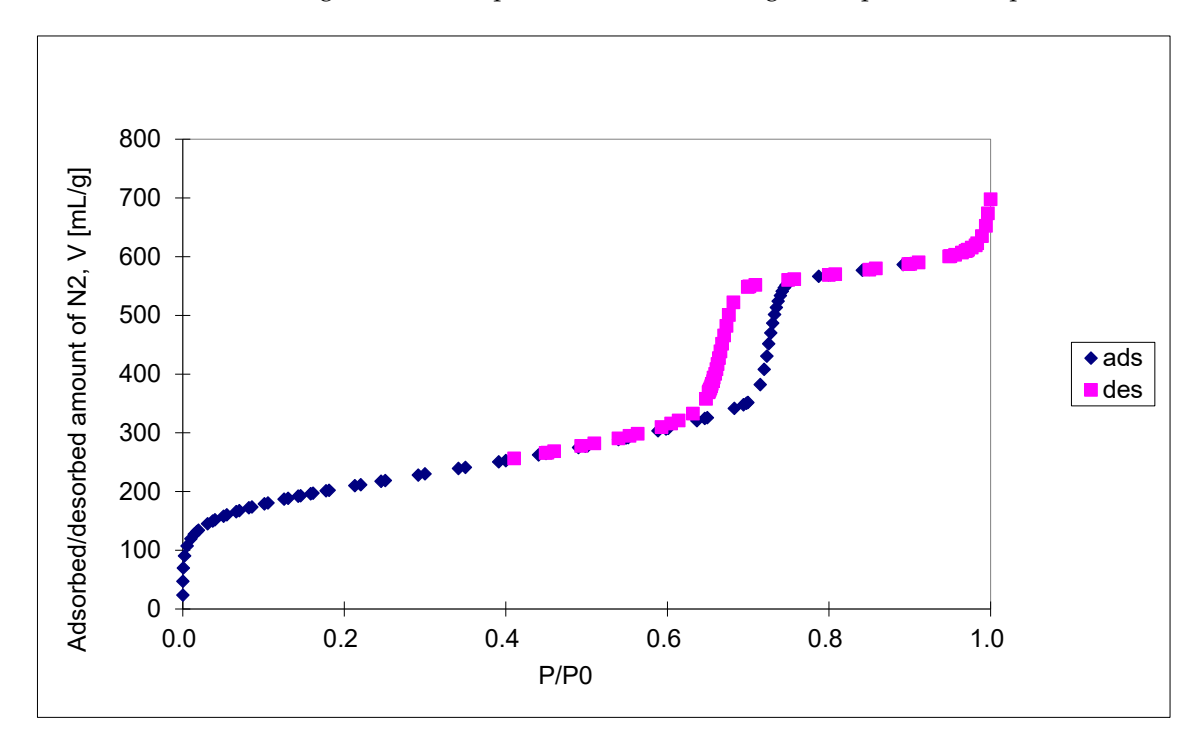


Figure 4. Nitrogen adsorption-desorption isotherms of calcined SBA-15.

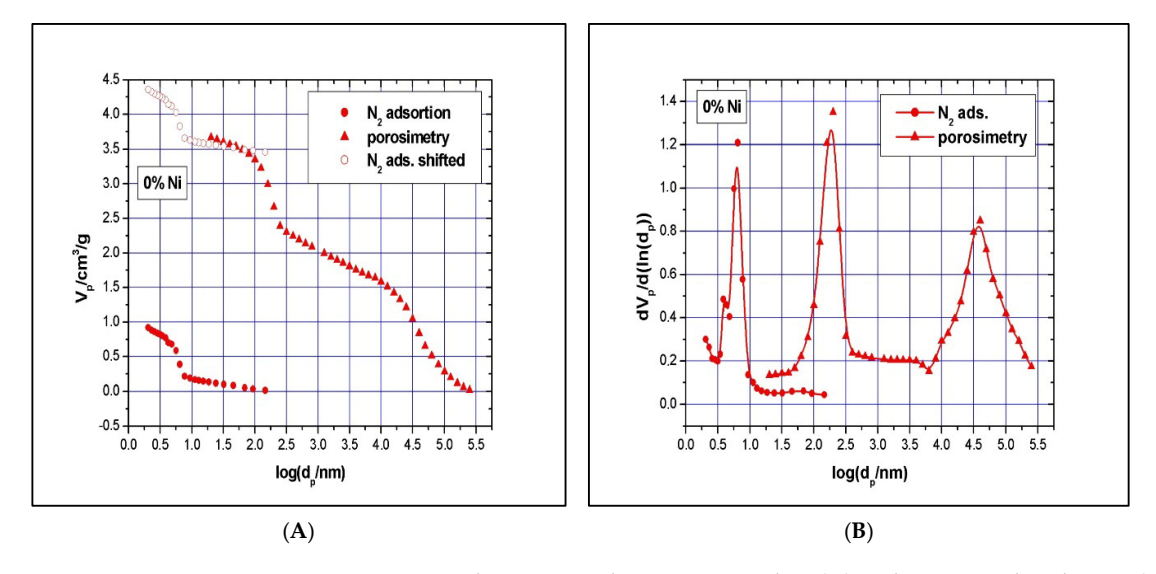


Figure 5. SBA-15 N₂-adsorption and Hg-intrusion data (A) and pore size distribution (B).

Using the XRD and BET measurements' results, the thickness of the pore walls was calculated as 3.2 nm (*thickness* = a - pore diameter). With these rather thick pore walls, the prepared SBA-15 sample is expected to have good mechanical and thermal resistance during the impregnation and calcination of the catalyst samples, and as such, the well-ordered structure is expected to be preserved.

3.2. Characterization Results of Catalysts

The well-ordered hexagonal structure was maintained by multi-step impregnation of nickel acetate into SBA-15. All samples displayed the three reflections: (100), (110), and (200), characteristic of the hexagonal array of mesochannels, although slightly shifted toward higher 2θ values as compared with the bare sample. The higher the loading, the higher the shift, and the higher the unit cell contraction. A possible interpretation of this result could be that some of the nickel was impregnated on the surface and not inside the silica framework. If this is the case, the volume of the pores for the catalyst samples should decrease as the loading is increased.

TEM/EDX revealed that the NiO wt% was 4.98 for the sample prepared through two impregnation cycles, while for the one with five impregnation cycles, the NiO wt% was 10.60. Therefore, the two samples were labeled as 5% Ni and 11% Ni, respectively.

A rough estimate of the NiO particle size can be derived from the TEM images. The particle size was between 1 and 3 nm.

The lack of crystallinity was also supported by the TeraHertz spectroscopy, performed both in ATR (Attenuated Total Reflectance) and Transmission modes. As shown in Figure 6, the spectra for both catalysts and the support are very similar. The lack of well-defined spectral features suggests that the crystallinity of the materials is close to zero. For sharp spectral features to exist, good long-range order and well-defined intermolecular bonding need to be present. Since this is absent in amorphous solids (i.e., SBA-15 spectrum), such samples tend to exhibit fewer spectral features, and if present, they tend to be broad in nature. By comparison, crystalline materials exhibit more spectral features, which are also much more defined than those observed in the amorphous phase. As the TeraHertz spectrum for the 11% Ni sample is broader than the one for the 5% Ni sample, the nickel oxide particles' size must be slightly larger than that for the sample with lower loading. Indeed, the higher the loading, the larger the size of the catalyst particles. To the best of our knowledge, this was the first time that TeraHertz spectroscopy has been applied to catalyst characterization.

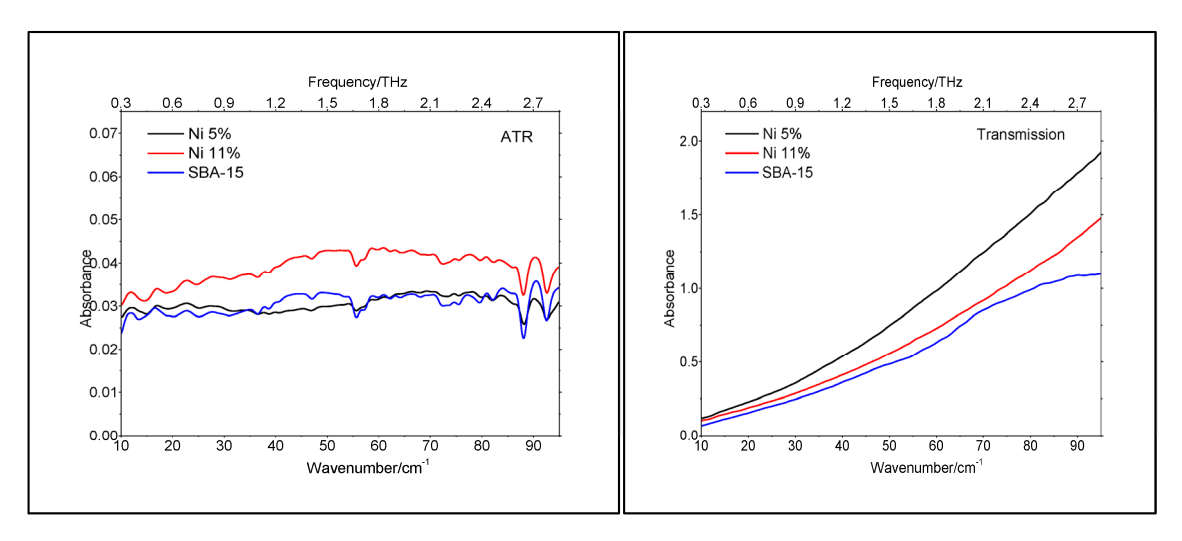


Figure 6. TeraHertz spectra of SBA-15 and catalyst samples.

Clear type IV with H1 hysteresis loop nitrogen physisorption curves, similar to the one of SBA-15, were observed. Although narrow pore size distributions were detected (see Figures 7 and 8), the main mesopore size decreased to about 2.6 nm, while the mesopores' volume decreased to about 0.74 cm³/g as the Ni loading was increased to 11%. The measured BET surface area was $547 \text{ m}^2/\text{g}$ for the 5% Ni sample and $506 \text{ m}^2/\text{g}$ for the 11%Ni one (Table 1). The significant reduction in specific surface area, pore volume, and size with increasing Ni loading implies some local blockage of the pore channel induced by depositing Ni species at the pore entrance or at the wall's surface and/or partial structural degradation, which can take place under higher Ni loading. The structural degradation can be assessed by calculating the dS/V number and comparing the value with the one obtained for SBA-15 above. For the 5% Ni sample, this number is 2.3, while for the 11% Ni sample is 1.8, clearly indicating that the structure suffered some degree of degradation if compared with SBA-15, for which the dS/V number is 4.3. If the impregnation led to the inclusion of nickel species in the wall by isomorphous substitution of silicon (Si⁴⁺ ion radius, 0.41 Å, Ni²⁺ ion radius, 0.69 Å) instead of unit cell contraction, an expansion would be observed. As the Hg-intrusion results show (Figures 7 and 8), there is a slight decrease in the macropores' diameter as well, especially for those in the region of 50–300 nm, and a broader size distribution, especially for macropores with a diameter in the 10–175 μm region. These changes are caused, in our opinion, by the deposition of nickel within the intra-particle voids as well.

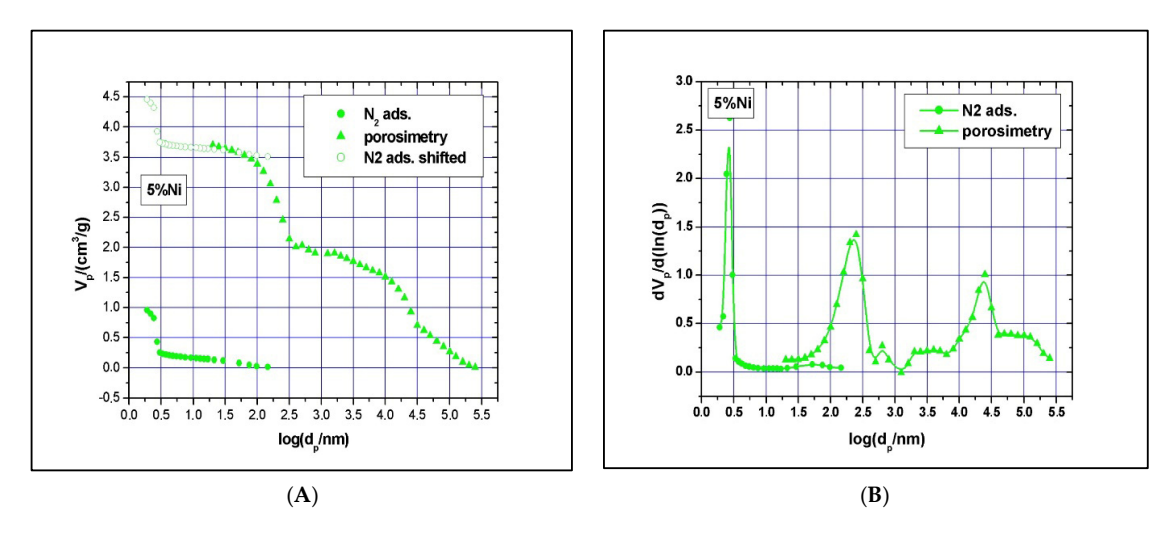


Figure 7. The 5% Ni N_2 -adsorption and Hg-intrusion data (A) and pore size distribution (B).

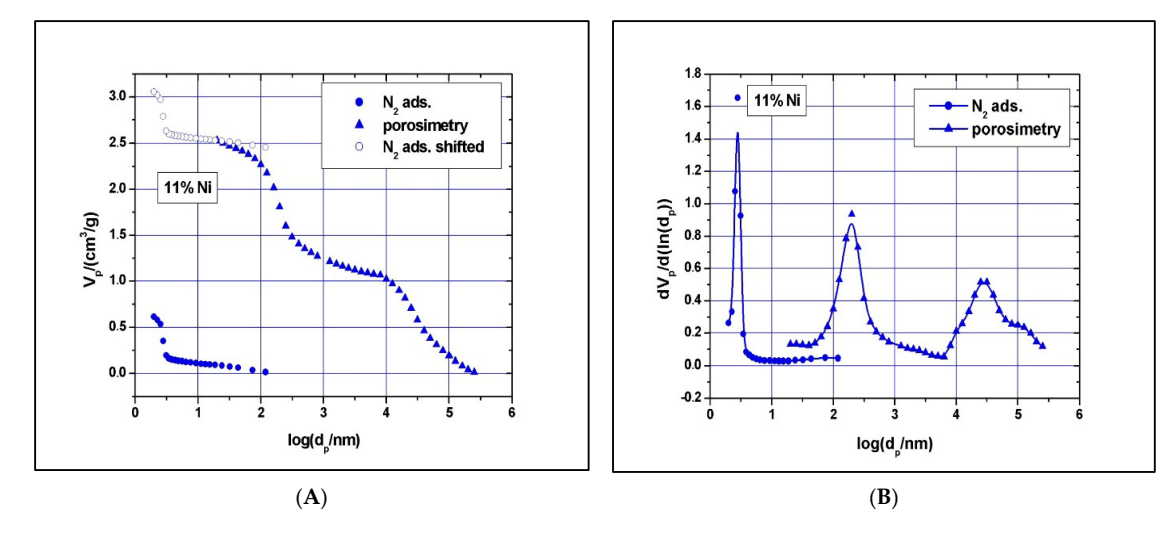


Figure 8. The 11% Ni N₂-adsorption and Hg-intrusion data (A) and pore size distribution (B).

Processes 2025, 13, 3505 11 of 22

TEM measurements over the two Ni samples (Figure 9) confirmed that the highly ordered mesoporous structure was maintained after the impregnation process and that the nickel species were uniformly distributed over the support, as XRD results have already revealed. Figure 9 shows the TEM micrograph of a selected area on the sample 5% Ni (A) and the chemical mapping of the same area (B, C, D). The TEM micrograph reveals that most of the nickel is located inside the pores. However, a small amount of nickel is present on the external surface. This means that the Ni oxide particles are larger than the diameter of the SBA-15 mesopore. TEM images for the 11% Ni sample were similar.

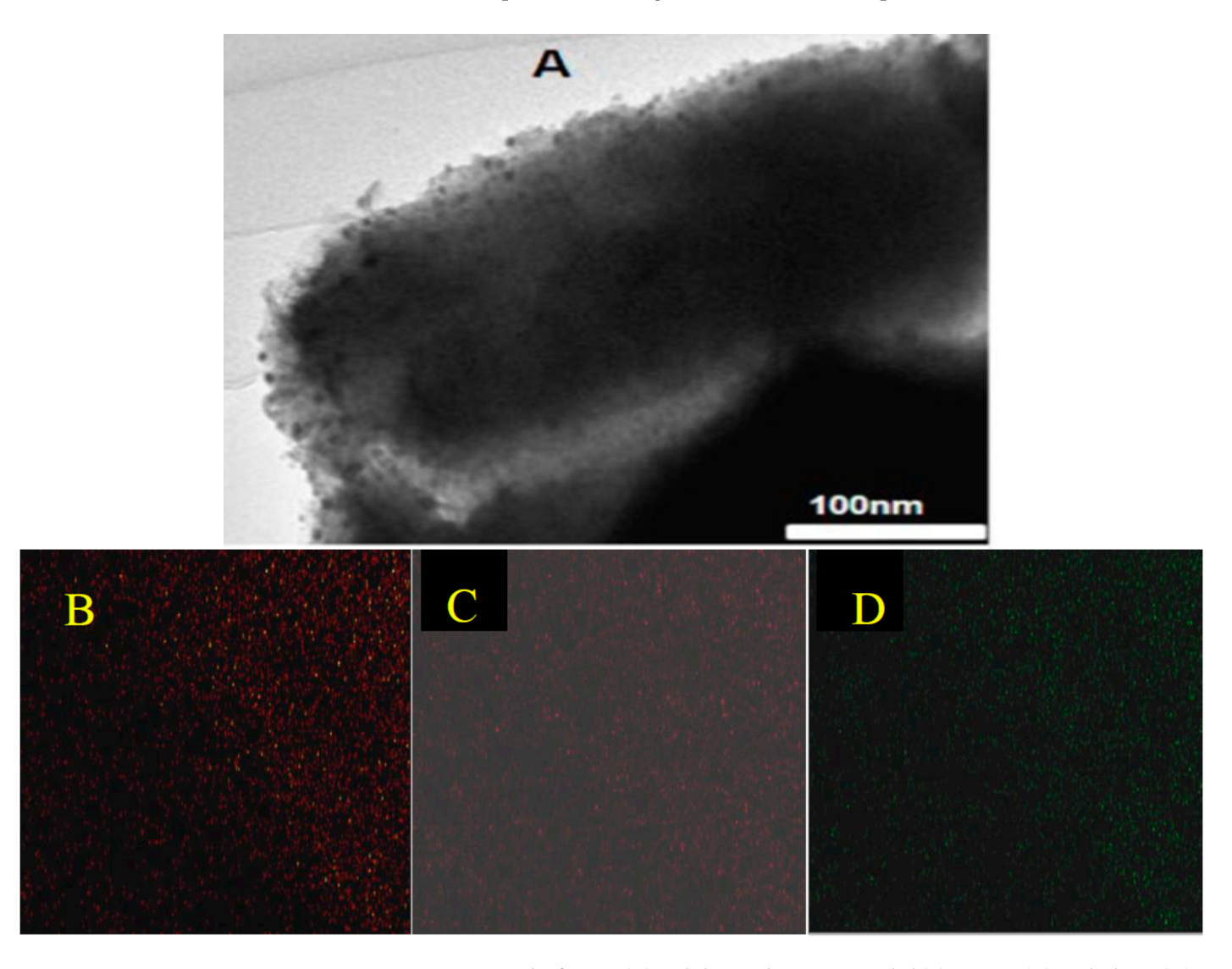


Figure 9. TEM micrograph of 5% Ni (A) and chemical mapping, nickel (B), oxygen (C), and silicon (D).

To further confirm the good dispersion of nickel oxide over the SBA-15 support, XPS measurements were performed for the two catalyst samples. Because of the high porosity of SBA-15, the depth with XPS is on the order of 5–10 nanometers (equivalent to 2–4 cylindrical pores). Figure 10 shows the XPS spectra for the Ni 2p region of the two as-synthesized samples, along with the spectra of the 5% Ni pre-reduced one. The main Ni peaks in the fresh samples are the Ni $2p_{3/2}$ peak at 856.1 eV and the Ni $2p_{1/2}$ at 874.5 eV, as well as their corresponding shake-up resonances at 863.1 and 880.2 eV. These peaks are assigned to oxidized nickel in a disperse phase [31]. From the XPS analysis, the atomic Ni/Si surface ratio was 0.13 for the 5% Ni sample and 0.17 for the 11% Ni one. From the EDX analysis, the atomic Ni/Si bulk ratios were 0.06 and 0.08, respectively. These results confirmed again

Processes 2025, 13, 3505 12 of 22

the dispersion of nickel species for both loadings, as the Ni/Si (surface) to Ni/Si (bulk) ratio is higher than 1. What is more, the XPS data obtained over the pre-reduced samples confirmed that the dispersion was not significantly altered by reduction; the Ni/Si ratio was 0.09 for the 5% Ni sample and 0.13 for the 11% Ni one.

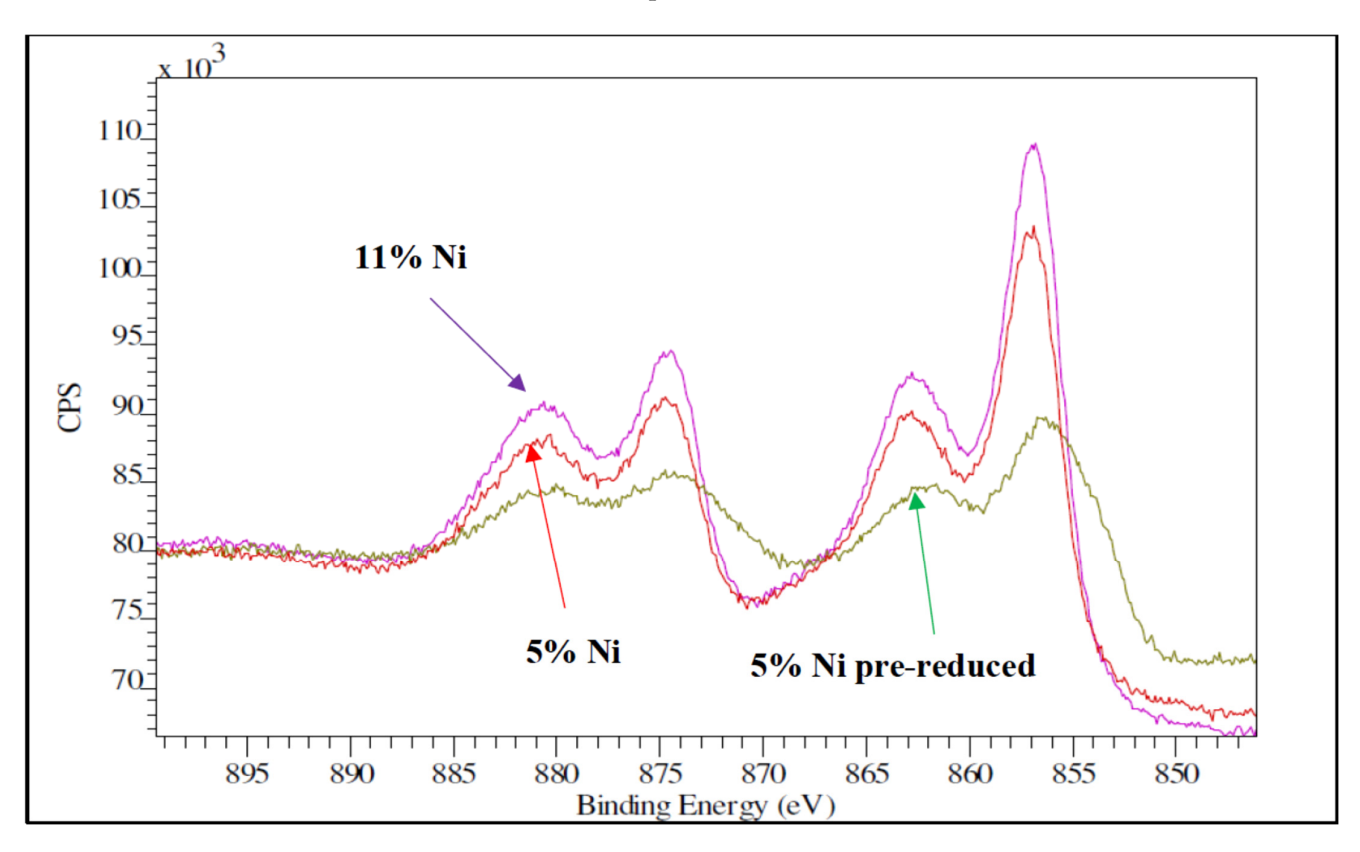


Figure 10. XPS spectra for Ni samples, fresh (5% Ni and 11% Ni) and pre-reduced (5% Ni).

Trying to comprehend even better the excellent dispersion of the nickel species over the support, we also looked at the influence of the impregnation and drying conditions on the metal distribution. It is generally understood that it is possible to control the structure, shape, and metal content when preparing heterogeneous catalysts by dry and wet impregnation. There are four main categories of metal profiles obtained by impregnation of the active phase into supports: uniform, egg-yolk, egg-shell, and egg-white. The choice of optimal metal profile in the support is determined by the required activity and selectivity, and by other characteristics of the chemical reactions (kinetics, mass transfer) [32].

For the dry reforming of methane application, we were interested in a uniform metal profile, as this profile proved to confer high activity and thermal stability of the catalyst. The ratio of the bulk solvent volume to the support volume has a significant effect on the metal distribution during the impregnation process, and this effect is more pronounced for wet impregnation than for dry support impregnation. But at the same time, this effect can be controlled and optimized by controlling the volume of the solvent. Therefore, the wet impregnation method was used in this study. Preliminary experiments concluded that using a bulk solvent volume: support volume ratio of 10–15:1 would result in a uniform metal profile. Consequently, a 13:1 ratio was used for this study. The precursor plays an important role as well in the active phase dispersion. We chose nickel acetate as a precursor because it was found that acetate has a stronger interaction with the support.

The concentration profile of the impregnated compound also depends on the mass transfer conditions within the support's pores during impregnation and drying. With this in mind, our choice for the SBA-15 as support was obvious. Using an optimized

Processes 2025, 13, 3505 13 of 22

method, SBA-15 with a high internal surface area and high thermal stability was prepared, as described below. Vacuum drying was chosen to avoid the collapse of the well-ordered mesoporous structure. In the case of mesoporous SBA-15, the impregnation solution should be easily sucked up by the mesoporous channels and generally fill the pores quickly, due to the capillary pressure [33]. However, as we expected that the SBA-15 support could lose some of its hydrophilicity by calcination, resulting in relatively low hydroxyl density, causing incomplete wetting and thus leading to inhomogeneous filling of pores during impregnation, the calcined SBA-15 sample was rehydrated in boiling water for 2 h.

The activity and selectivity toward the dry reforming of the methane reaction of the two nickel samples were tested via temperature programmed reaction (TPRx), with the $CH_4:CO_2=1.5:1$ mixtures. As shown in Figure 11A,B for the 5% Ni sample and Figure 12A,B for the 11% Ni one, both fresh (as-synthesized) and pre-reduced catalyst samples proved to be very active.

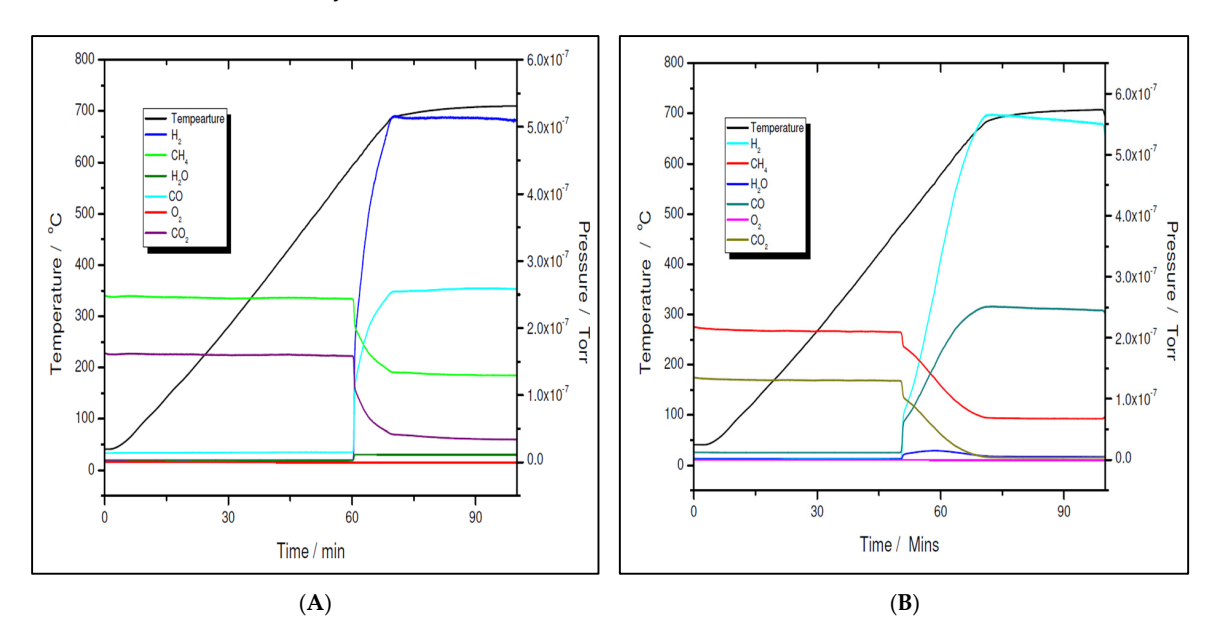


Figure 11. Temperature programmed reaction over 5% Ni fresh (A) and 5% Ni pre-reduced (B).

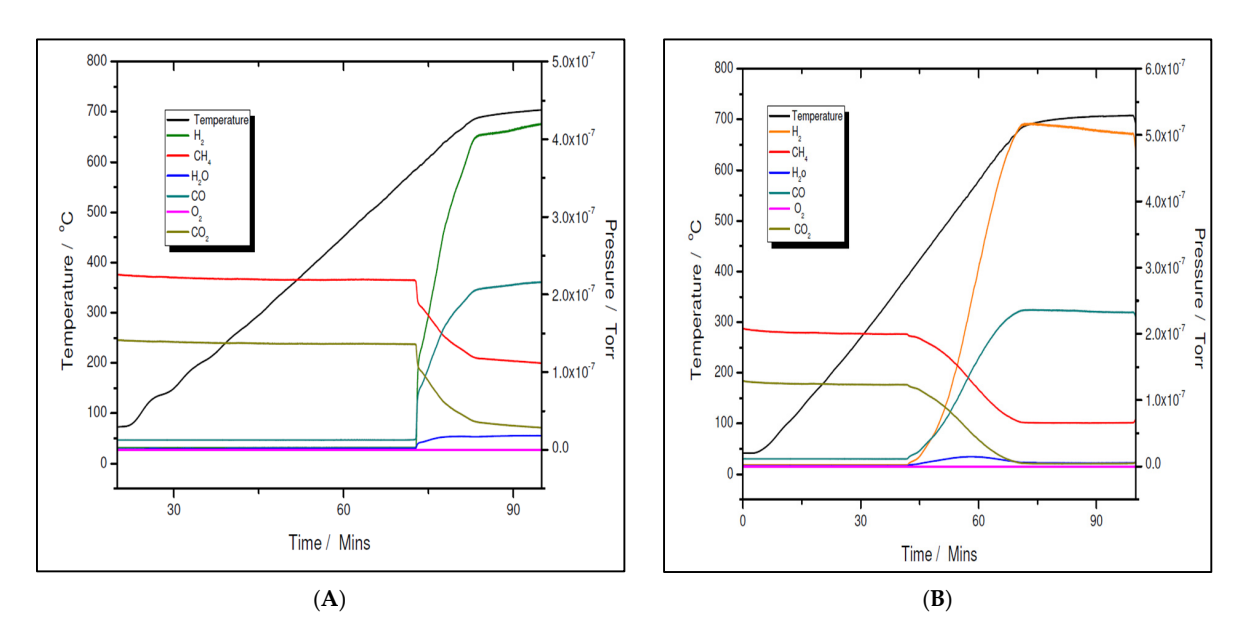


Figure 12. Temperature programmed reaction over 11% Ni fresh (A) and 11% Ni pre-reduced (B).

Processes 2025, 13, 3505 14 of 22

However, for both loadings, the pre-reduced samples were more active than the fresh ones. For example, for the 5% Ni loading, the pre-reduced sample starts to produce H_2 and CO at 480 °C, while the fresh one must exceed 600 °C to start to convert the reactants. While for the pre-reduced sample, almost complete CO₂ conversion, e.g., higher than 99%, was obtained at approximately 680 °C, for the fresh one, only 75% CO₂ conversion was obtained at this temperature. A slightly improved catalytic activity was observed for both 11% loading samples. The fresh 11% Ni sample starts to convert the reactants at approximately 580 °C, while for the pre-reduced sample, the reaction was initiated at temperatures as low as 380 °C with CO₂ conversion higher than 99% at the same temperature as that for the 5% Ni pre-reduced sample, i.e., 680 °C. The CO₂ conversion over the fresh sample at 680 °C was the same as for the fresh 5% Ni sample. Therefore, the only difference in activity between the two catalysts was in terms of their initial activity. The 11% Ni pre-reduced sample was slightly more active as it starts to convert the reactants at 380 °C, about 100 °C less than the 5% Ni pre-reduced one. Obviously, by increasing the Ni loading, the number of active sites increased, which explains the earlier start of the reaction over the 11% Ni pre-reduced sample. However, as the maximum performance was obtained at the same temperature for both pre-reduced samples, one can conclude that the active species/sites were the same for both loadings.

A more careful analysis of the TPRx data (Figures 11 and 12) revealed that, while CH_4 and CO_2 are not adsorbed on the fresh catalysts at temperatures lower than the starting reaction temperatures, for the pre-reduced samples, some adsorption (about 5 mol% of both CH_4 and CO_2) is noticed as the samples are heated up.

These results were confirmed by the TAP measurements as well. As previously reported [34], over the fresh 5% Ni sample, both CH_4 and CO_2 were only weakly and reversibly adsorbed at temperatures lower than $600\,^{\circ}$ C. Additional TAP measurements were performed over the pre-reduced 5% Ni sample, while single pulses of a $CH_4:CO_2 = 1.5:1$ mixture were sent over the catalyst, at temperatures varying between room temperature and $600\,^{\circ}$ C. The results are presented in Figure 13A–C. It seems that CO_2 is physically adsorbed at low temperatures and slightly chemisorbed at high temperatures, while CH_4 is only slightly chemisorbed at high temperatures. At $600\,^{\circ}$ C, a broader peak CO_2 response was observed, suggesting that the CO_2 interaction with catalysts was stronger than the CH_4 one.

As the TPRx data revealed, both catalyst samples are very active. The well dispersion of the nickel species over the support was, in our opinion, responsible for their very high activity. To the best of our knowledge, no Ni-based catalysts with almost complete CO_2 conversion at temperatures lower than 800 °C have been reported so far. Although Ni/SBA-15 catalysts have been already reported [29,35], their catalytic activity toward the DRM reaction was much lower than that of the samples of this study. For example, the CO_2 conversion at 700 °C was between 68% and 75%, as the Ni loading increased from 2.5% to 20%. For a 5% Ni/SBA-15 catalyst, prepared by the wet impregnation method (same as the one used in this study) but using nickel nitrate as Ni precursor, the reported CO_2 conversion at 700 °C is 65% [36]. It is clear evidence of the effect of the Ni precursor. And, as mentioned above, the nature of the precursor is one of the factors responsible for the Ni dispersion. To understand why and how the Ni dispersion is affected by the nature of the precursor, we took a deeper look at the drying process during the catalyst's preparation.

Processes 2025, 13, 3505 15 of 22

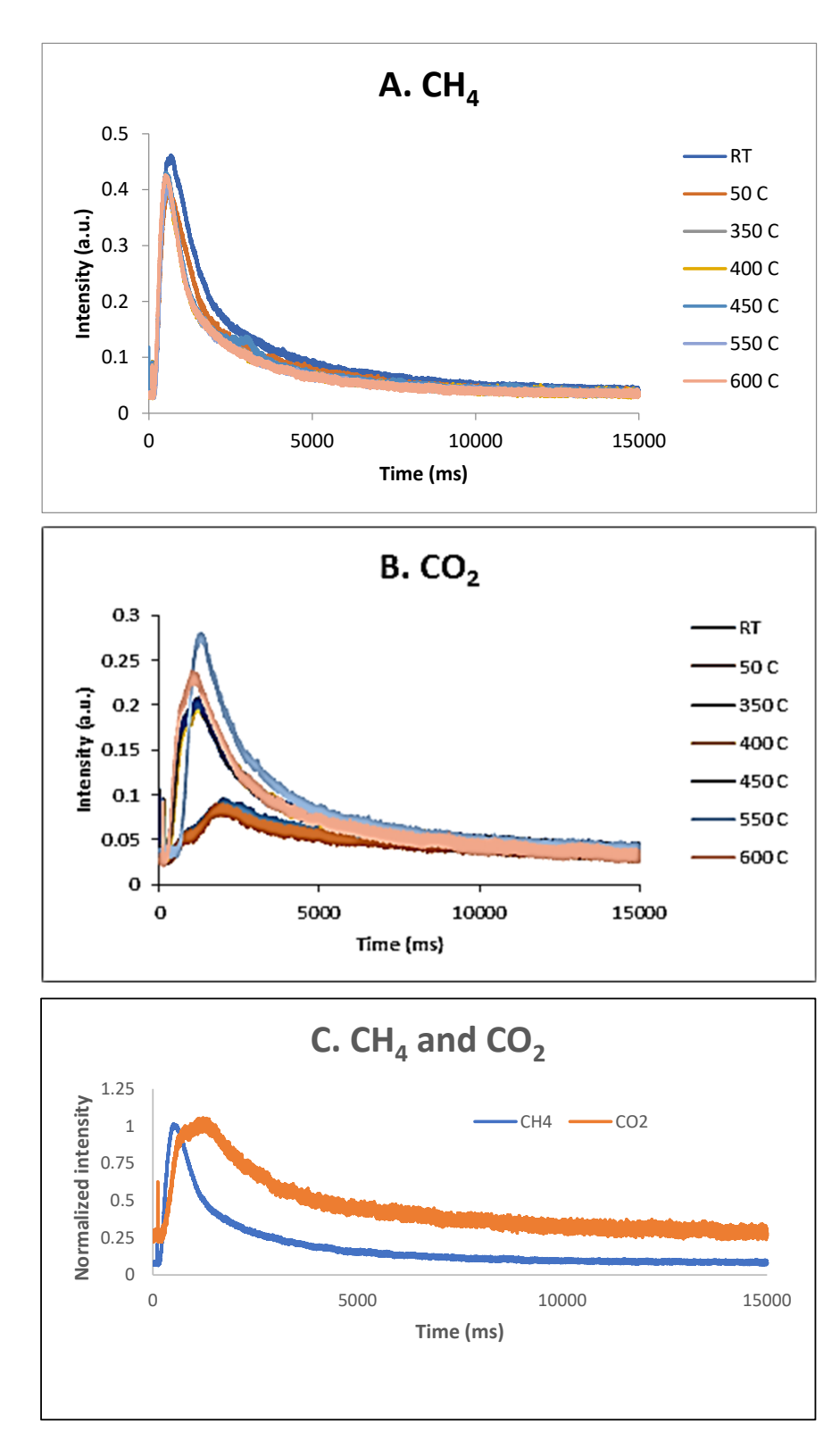


Figure 13. CH₄ (**A**) and CO₂ (**B**) response to single-pulse experiments with a CH₄:CO₂ = 1.5:1 mixture over pre-reduced 5% Ni sample at temperatures from RT to 600 $^{\circ}$ C; (**C**) CH₄ and CO₂ intensity normalized responses at 600 $^{\circ}$ C.

In accordance with the literature data [33], the physical picture of drying can be described as follows: as drying proceeds, the solution of the precursor with low surface tension could diffuse deeply at first and be transported toward the internal surface of the mesoporous channels via capillary forces; toward the end of drying, the enhanced viscosity could lead to a strong interaction with the internal surface of the support and inhibit

the redistribution of the impregnation solution during drying, thus favoring a uniform distribution of the active component in the mesoporous channels. In contrast, the solution of the precursor with higher surface tension has a weak interaction with the support, and the concentrated solvent sucked up by the mesoporous pores could be back diffused by the higher surface tension and migrate toward the external surface of the mesoporous channels, resulting in a concentration build-up on the external rim of the support. As a consequence, inhomogeneous distributions of the precursor appeared. Knowing that the surface tension of acetic acid is lower than that of nitric acid, i.e., 0.028 N/m compared to 0.04115 N/m at 20 °C [37,38], our choice of nickel acetate tetrahydrate as the Ni precursor was obvious, and homogeneous impregnation was obtained as expected.

Although the prepared catalyst samples proved to be very active at low temperatures, there was another challenge to address. As seen in Figures 11 and 12, the amount of hydrogen produced was almost double the amount of carbon dioxide. This means that in addition to the main reaction, the catalysts favored the methane decomposition as well, which, unfortunately, might have led to the carbon deposition over the surface, and in time, to the deactivation of catalyst (not seen in the above figures). On the other hand, small amounts of water were noticed as well. This can be ascribed to the simultaneous occurrence of the reverse water-gas shift reaction. To support these assumptions, temperature programmed CH₄ decomposition (reduction) (Figures 14A and 15A) followed by temperature programmed oxidation (TPO) (Figures 14B and 15B) measurements were also performed on both fresh samples. For both samples, the methane activation reaches its maximum at 580 °C. The TPO measurements showed that for both samples, three CO₂ peaks are present, meaning that three carbon species were formed during methane decomposition. Along with carbon dioxide, some carbon monoxide was formed and was almost constant, though higher for the 5% Ni sample, and an amount of water was also released. The formation of CO indicates that the carbon species, formed by the dissociation of CH₄, react rapidly with oxygen species from the catalyst. This is another evidence that the presence of carbonaceous species will not contribute to the catalyst's deactivation.

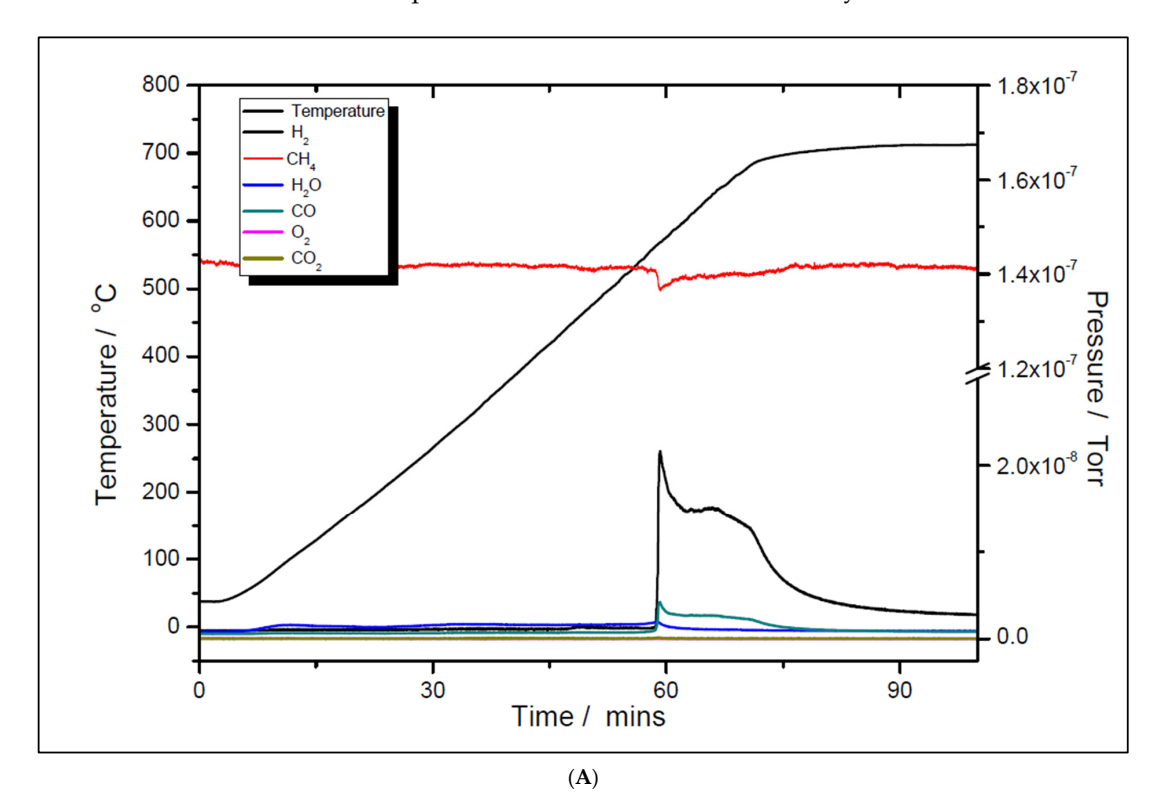


Figure 14. Cont.

Processes 2025, 13, 3505 17 of 22

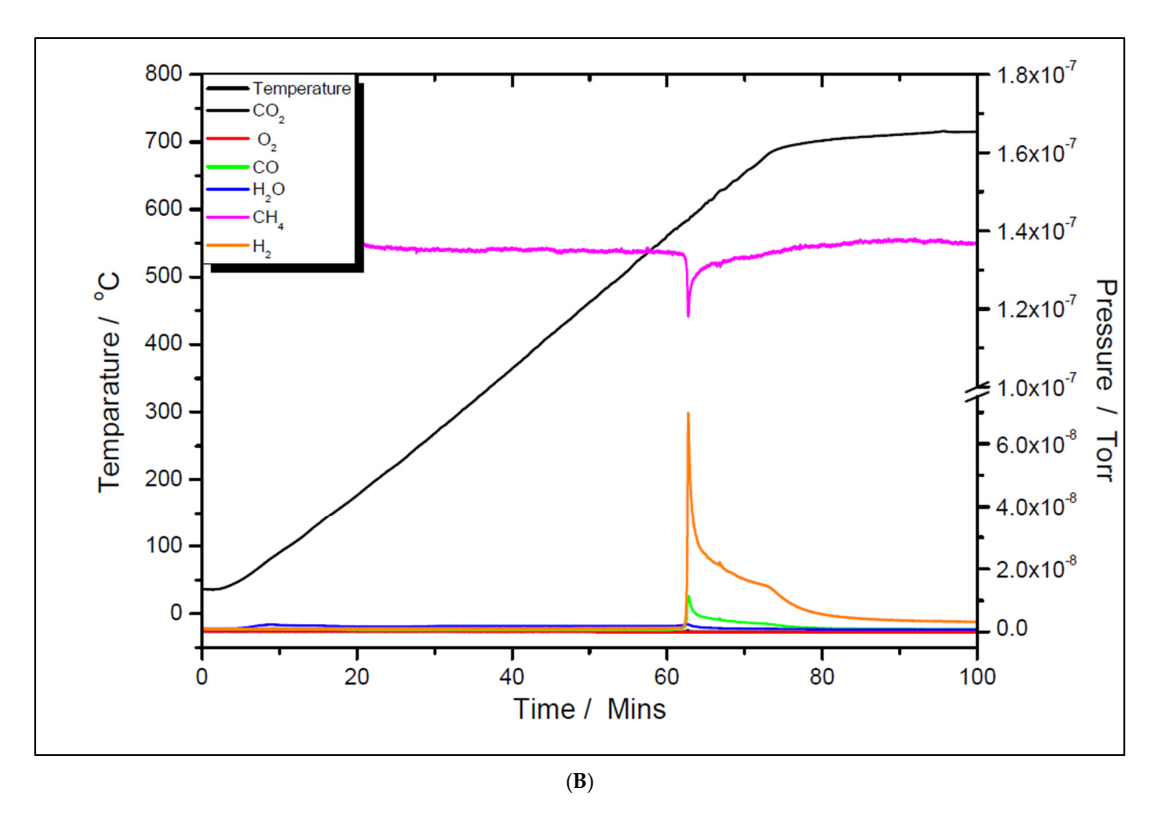


Figure 14. Temperature programmed CH₄ decomposition (reduction) over 5% Ni (A) and 11% Ni (B).

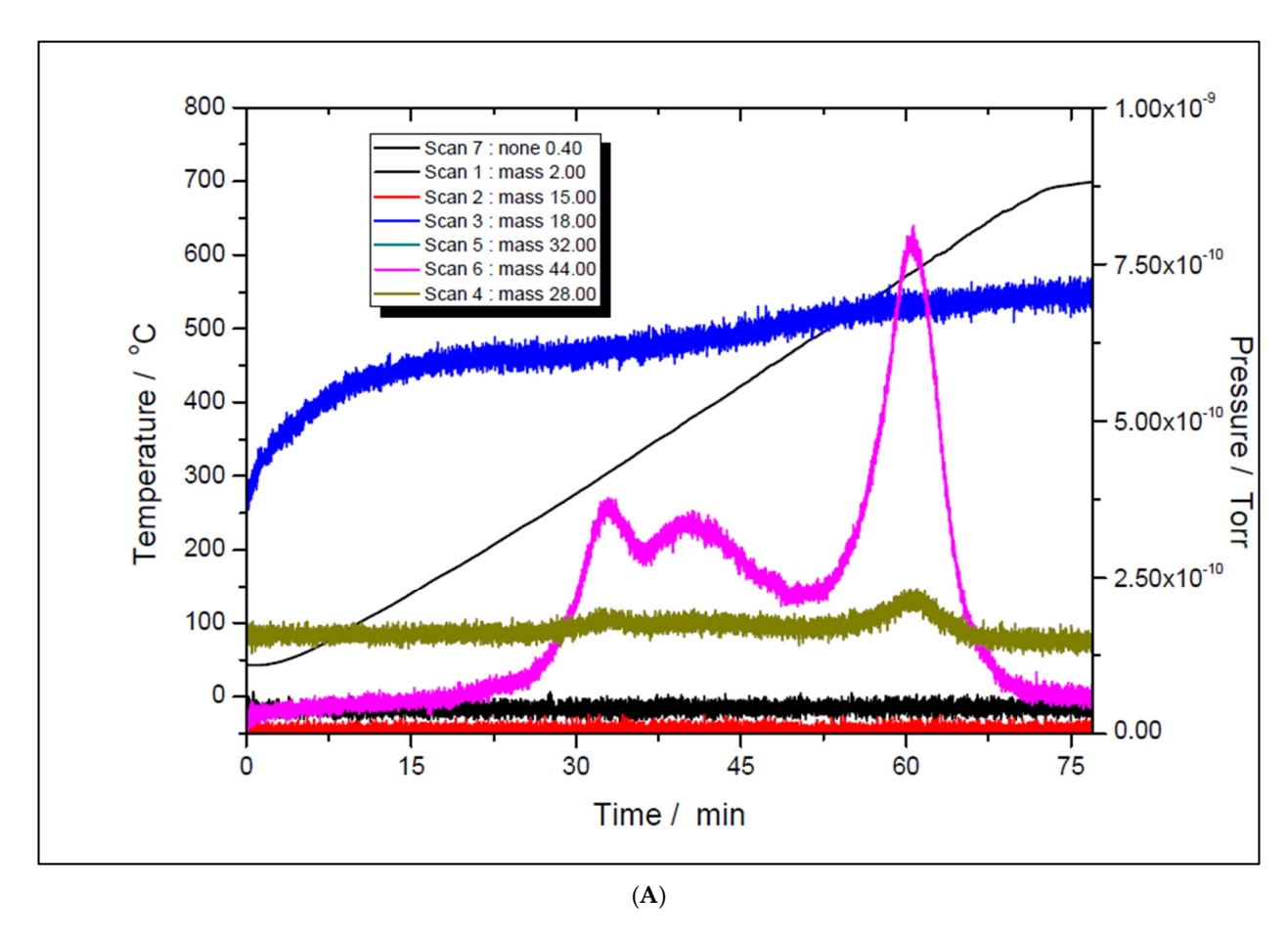


Figure 15. Cont.

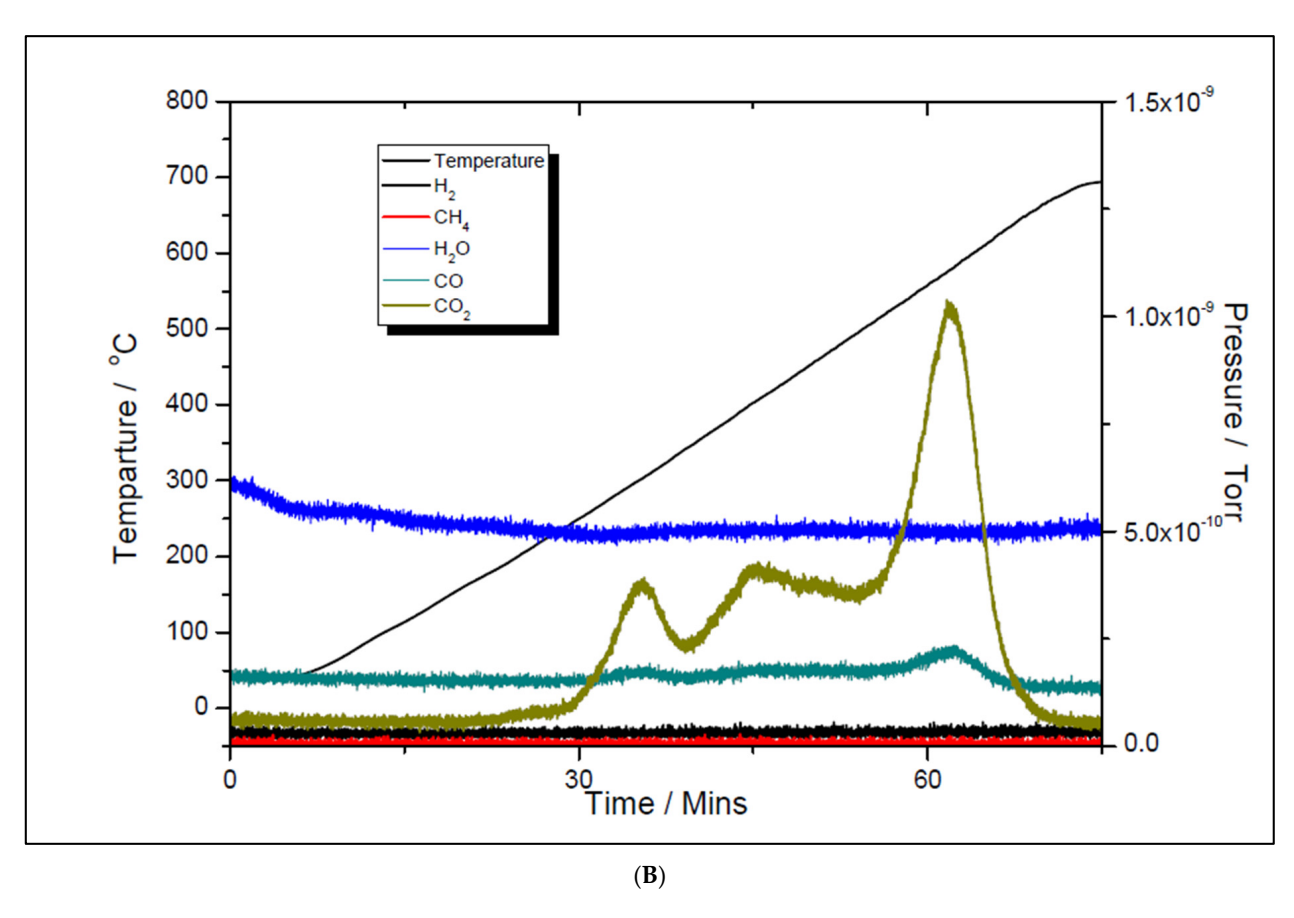


Figure 15. Temperature programmed oxidation to recover carbon from the surface of 5% Ni (**A**) and 11% Ni (**B**).

The three surface carbon species, labeled as C_{α} , C_{β} , and C_{γ} , respectively, showed various mobility, thermal stability, and reactivity [36]. The peaks' temperatures were the same for both Ni loadings, i.e., 280, 400, and 580 °C, respectively. The distribution and features of these carbonaceous species sensitively depend on the nature of the transition metals and the conditions of methane adsorption. These carbonaceous species can be described as: completely dehydrogenated carbidic C_{α} type, partially dehydrogenated CH_{x} $(1 \le x \le 3)$ species, namely C_{β} type, and carbidic clusters C_{γ} type (formed by the agglomeration and conversion of C_{α} and C_{β} species under certain conditions). Their reactivity was assessed by performing TPSR with hydrogen [35]. Similar results to those obtained from TPO measurements in this study were obtained. A fraction of the surface carbon species, which might be assigned to carbidic C_{α} (~188 °C), were mainly hydrogenated to methane at temperatures even below 227 °C. This showed that carbidic C_{α} species are rather active and thermally unstable on the nickel surface. The carbidic C_{α} species were suggested to be responsible for CO formation. A significant number of surface carbon species were hydrogenated to methane below 327 °C and were assigned to partially dehydrogenated C_{β} species. Most of the surface carbon was hydrogenated above 527 °C and was attributed to carbidic clusters $C\gamma$ [39].

As all three carbonaceous species were rather active, being converted to carbon dioxide at temperatures lower than the starting temperature of CO_2 reforming, one can assume that they will not contribute to the catalyst deactivation. To support this statement, post-reaction temperature-programmed oxidation (TPO) experiments were carried out by exposing the spent catalysts to 5% oxygen in helium flow in order to determine the amount of carbon formed during the DRM reaction and run for 200 min at 600 $^{\circ}$ C. No CO_2 peaks were observed for either of the samples. In addition, in this TPO experiment, there was no signal

for water, which was in line with previous work [40]. What is more, a transient study on the dry reforming of methane showed that when both reactants are fed contemporaneously, the presence of CH_X species promotes the CO_2 activation that is responsible for the reforming reaction [41]. Our understanding is that the uniform distribution of the metal component throughout the oxide support with high surface area helped to reduce coking by physically separating carbon species formed on the nickel surface. That is, carbon species must be formed if the main reaction is to proceed, but prevention of polymerization by separating the carbon species should reduce coking while leaving the main reaction unaffected [42].

There is another important factor that contributes to the stability of the Ni-based catalysts [43]. As the dry reforming reaction typically occurs at very high temperatures, the initially small Ni particles become sintered, and the size of the Ni domains eventually becomes large with heavy coke deposition.

Strong metal-support interactions are often used to maintain the small size of the Ni particles at high reaction temperatures. A way to quantify the metal-support interactions is to study the kinetics of the H_2 -reduction of the calcined samples. For the catalysts prepared using nickel nitrate as a precursor, the activation energy for the reduction process decreased as the Ni-loading increased, which means that the metal-support interaction is stronger at lower Ni loading [44]. Accordingly, less carbon deposition should occur on the catalysts with lower Ni loading as compared with those with higher loading. Another variable with significant influence on catalyst activity and the amount of coke is the support material. The activity and stability of the 5 wt% Ni/SBA-15 catalyst sample was assessed against those of a benchmark catalyst, i.e., commercial Ni/Al₂O₃ catalyst, which was bought from a reputable catalysts manufacturer and was characterized by the same techniques and tested for the dry reforming of methane reaction (with permission from the manufacturer), in the same experimental set-up as the catalyst developed by us. Details of this assessment can be found in Supplementary Materials—Comparison. In brief, the comparison showed that the physical characteristics, such as the hydrothermal stability of the catalyst support, high surface area of the catalyst with thick-walled pore channels, small size of nickel particles, and high dispersion of nickel onto the support, were mainly responsible for the higher activity and stability of the Ni/SBA-15 catalyst compared to the Ni/Al₂O₃ catalyst. Although the Ni/Al₂O₃ catalyst also had small nickel particles with strong metal-support interaction, its low surface area, non-porous support, and poor dispersion of nickel on the alumina support were major setbacks that inhibited its catalytic activity and stability in DRM.

4. Conclusions

Two highly ordered Ni-based catalyst samples have been prepared, their physical properties assessed, and their catalytic activity tested toward the reforming of methane with carbon dioxide in their as-synthesized and as pre-reduced forms. The two Ni catalyst samples, namely 5% Ni and 11% Ni, supported on the sol-gel made from SBA-15 mesoporous silica using an optimized preparation method and nickel acetate tetrahydrate as Ni precursor, have shown high and almost identical catalytic activity for CO_2 reforming of methane to synthesis gas, with the 11% Ni sample having a slightly improved activity. Significant catalytic activity can be obtained at temperatures as low as 450 °C. The catalysts in their pre-reduced forms have shown higher activities compared to the as-synthesised (fresh) ones.

Along with the high activity, the two catalyst samples proved to have high coking resistivities. Their outstanding performance and coking resistivities have been found to be closely related to the very small size of Ni particles and their high dispersion over the high BET surface area support.

Processes 2025, 13, 3505 20 of 22

Due to their high coking resistivity and complete CO_2 conversion at temperatures lower than their deactivation temperatures and for a $CH_4:CO_2$ ratio closer to the one in biogas, i.e., 1.5:1, these catalysts are suitable for scaling-up to a sustainable DRM commercial technology, with high impact at economic, environmental, and societal levels.

Their suitability for sustainable DRM commercial technology was successfully confirmed in a pilot plant. The Ni/SBA-15 catalysts were shaped into pellets by extrusion, using methyl cellulose and colloidal silica as binders. And tested in a pyrolysis pilot plant fitted with a catalytic reactor for sewage sludge pyrolysis tar removal. The Ni/SBA-15 catalyst pellets remained highly active and stable throughout the test's duration, converting 100% tar in the hot gas to smaller non-condensable gases, thereby increasing the pyrolysis gas fraction and eliminating the problematic tar in the vapor stream. Pilot plant tests revealed that the catalyst pellets were able to crack 100% of tar into hydrogen, carbon monoxide, and methane [45].

Supplementary Materials: The following supporting information can be downloaded at: https://www.mdpi.com/article/10.3390/pr13113505/s1.

Author Contributions: Conceptualization, M.O. and T.S.; Methodology, M.O. and T.S.; Validation, T.S.; Formal analysis, M.O.; Investigation, M.O. and T.S.; Writing—original draft, M.O. All authors have read and agreed to the published version of the manuscript.

Funding: This research received no external funding.

Data Availability Statement: Data is unavailable due to privacy restrictions.

Acknowledgments: We thank David Reece for the TeraHertz spectroscopy measurements, David Lundie from Hiden Analytical for some preliminary Catlab measurements, Nouria Fatah for Mercury porosimetry, and Wei Wang for useful discussions regarding the preparation of mesoporous materials.

Conflicts of Interest: The authors declare no conflict of interest.

References

- 1. Bradford, M.C.J.; Vannice, M.A. Catalytic reforming of methane with carbon dioxide over nickel catalysts I. Catalyst characterization and activity. *Appl. Catal. A* **1996**, *142*, 73–96. [CrossRef]
- 2. van Keulen, A.N.J.; Seshan, K.; Hoebink, J.H.B.J.; Ross, J.R.H. TAP Investigations of the CO₂ Reforming of CH₄ over Pt/ZrO₂. *J. Catal.* **1997**, *166*, 306–314. [CrossRef]
- 3. Chytil, S.; Haugland, L.; Blekkan, E.A. On the mechanical stability of mesoporous silica SBA-15. *Microporous Mesoporous Mater.* **2008**, *111*, 134–142. [CrossRef]
- 4. Wang, R.; Xu, H.; Liu, X.; Ge, Q.; Li, W. Role of redox couples of $Rh^0/Rh^{\delta+}$ and Ce^{4+}/Ce^{3+} in CH_4/CO_2 reforming over $Rh-CeO_2/Al_2O_3$ catalyst. *Appl. Catal. A* **2006**, *305*, 204–210. [CrossRef]
- 5. Nematollahi, B.; Rezaei, M.; Khajenoori, M. Combined dry reforming and partial oxidation of methane to synthesis gas on noble metal catalysts. *Int. J. Hydrogen Energy* **2011**, *36*, 2969–2978. [CrossRef]
- 6. Tao, K.; Zhang, Y.; Terao, S.; Tsubaki, N. Development of platinum-based bimodal pore catalyst for CO₂ reforming of CH₄. *Catal. Today* **2010**, *153*, 150–155. [CrossRef]
- 7. Tao, K.; Zhang, Y.; Terao, S.; Yoneyama, Y.; Kawabata, T.; Matsuda, K.; Ikeno, S.; Tsubaki, N. Chemical and spatial promotional effects of bimodal pore catalysts for methane dry reforming. *Chem. Eng. J.* **2011**, *170*, 258–263. [CrossRef]
- 8. Pan, Y.-X.; Liu, C.-J.; Shi, P. Preparation and characterization of coke resistant Ni/SiO₂ catalyst for carbon dioxide reforming of methane. *J. Power Sources* **2008**, *176*, 46–53. [CrossRef]
- 9. Al-Fatish, A.S.A.; Ibrahim, A.A.; Fakeeha, A.H.; Soliman, M.A.; Siddiqui, M.R.H.; Abasaeed, A.E. Coke formation during CO₂ reforming of CH₄ over alumina-supported nickel catalysts. *Appl. Catal. A* **2009**, *364*, 150–155. [CrossRef]
- 10. Tian, L.; Zhao, X.; Liu, B.S.; Zhang, W. Preparation of an Industrial Ni-Based Catalyst and Investigation on CH₄/CO₂ Reforming to Syngas. *Energy Fuels* **2009**, 23, 607–612. [CrossRef]
- 11. Rivas, I.; Alvarez, J.; Pietri, E.; Pérez-Zurita, M.J.; Goldwasser, M.R. Perovskite-type oxides in methane dry reforming: Effect of their incorporation into a mesoporous SBA-15 silica-host. *Catal. Today* **2010**, *149*, 388–393. [CrossRef]
- 12. Xu, J.; Zhou, W.; Li, Z.; Wang, J.; Ma, J. Biogas reforming for hydrogen production over a Ni–Co bimetallic catalyst: Effect of operating conditions. *Int. J. Hydrog. Energy* **2010**, *35*, 13013–13020. [CrossRef]

Processes 2025, 13, 3505 21 of 22

13. Huang, T.; Huang, W.; Huang, J.; Ji, P. Methane reforming reaction with carbon dioxide over SBA-15 supported Ni–Mo bimetallic catalysts. *Fuel Process. Technol.* **2011**, 92, 1868–1875. [CrossRef]

- 14. Foo, S.Y.; Cheng, C.K.; Nguyen, T.-H.; Adesina, A.A. Kinetic study of methane CO₂ reforming on Co–Ni/Al₂O₃ and Ce–Co–Ni/Al₂O₃ catalysts. *Catal. Today* **2011**, *164*, 221–226. [CrossRef]
- 15. Wang, N.; Chu, W.; Zhang, T.; Zhao, X.S. Synthesis, characterization and catalytic performances of Ce-SBA-15 supported nickel catalysts for methane dry reforming to hydrogen and syngas. *Int. J. Hydrog. Energy* **2012**, *37*, 19–30. [CrossRef]
- 16. Li, X.; Hu, Q.; Yang, Y.; Wang, Y.; He, F. Studies on stability and coking resistance of Ni/BaTiO₃–Al₂O₃ catalysts for lower temperature dry reforming of methane (LTDRM). *Appl. Catal. A* **2012**, *413*–414, 163–169. [CrossRef]
- 17. Bartholomew, C.H. Mechanisms of catalyst deactivation. Appl. Catal. A 2001, 212, 17-60. [CrossRef]
- 18. Matsumura, Y.; Nakamori, T. Steam reforming of methane over nickel catalysts at low reaction temperature. *Appl. Catal. A* **2004**, 258, 107–114. [CrossRef]
- 19. Cai, Y.; Zhang, Y.; Zhang, X.; Wang, Y.; Zhao, Y.; Li, G.; Zhang, G. Recent advances in Ni-based catalysts for CH₄-CO₂ reforming (2013–2023). *Atmosphere* **2023**, *14*, 1323. [CrossRef]
- 20. Koo, K.Y.; Roh, H.-S.; Seo, Y.T.; Seo, D.J.; Yoon, W.L.; Bin Park, S. A highly effective and stable nano-sized Ni/MgO–Al₂O₃ catalyst for gas to liquids (GTL) process. *Int. J. Hydrog. Energy* **2008**, *33*, 2036–2043. [CrossRef]
- 21. Bradford, M.C.J.; Vannice, M.A. CO₂ Reforming of CH₄. Catal. Rev. Sci. Eng. 1999, 41, 1–42. [CrossRef]
- 22. Zhang, S.; Wang, J.; Liu, H.; Wang, X. One-pot synthesis of Ni-nanoparticle-embedded mesoporous titania/silica catalyst and its application for CO₂-reforming of methane. *Catal. Commun.* **2008**, *9*, 995–1000. [CrossRef]
- 23. Kaydouh, M.-N.; El Hassan, N.; Davidson, A.; Casale, S.; El Zakhem, H.; Massiani, P. Effect of the order of Ni and Ce addition in SBA-15 on the activity in dry reforming of methane. *C.R. Chim.* **2015**, *18*, 293–301. [CrossRef]
- 24. Zhao, D.; Huo, Q.; Feng, J.; Chmelka, B.F.; Stucky, G.D. Nonionic Triblock and Star Diblock Copolymer and Oligomeric Surfactant Syntheses of Highly Ordered, Hydrothermally Stable, Mesoporous Silica Structures. *J. Am. Chem. Soc.* 1998, 120, 6024–6036. [CrossRef]
- Zhao, D.; Feng, J.; Huo, Q.; Melosh, N.; Fredrickson, G.H.; Chmelka, B.F.; Stucky, G.D. Triblock Copolymer Syntheses of Mesoporous Silica with Periodic 50 to 300 Angstrom Pores. Science 1998, 279, 548–552. [CrossRef]
- 26. Olea, M.; Kunitake, M.; Shido, T.; Asakura, K.; Iwasawa, Y. Temporal Analysis of Products (TAP) Study of the Adsorption of CO, O₂, and CO₂ on a Au/Ti(OH)₄* Catalyst. *Bull. Chem. Soc. Jpn.* **2001**, 74, 255–265. [CrossRef]
- 27. Holmqvist, P.; Alexandridis, P.; Lindman, B. Modification of the Microstructure in Block Copolymer—Water—"Oil" Systems by Varying the Copolymer Composition and the "Oil" Type: Small-Angle X-ray Scattering and Deuterium-NMR Investigation. *J. Phys. Chem. B* **1998**, *102*, 1149–1158. [CrossRef]
- 28. Eliche-Quesada, D.; Merida-Robles, J.; Maireles-Torres, P.; Rodriguez-Castellon, E.; Jimenez-Lopez, A. Hydrogenation and Ring Opening of Tetralin on Supported Nickel Zirconium-Doped Mesoporous Silica Catalysts. Influence of the Nickel Precursor. *Langmuir* 2003, 19, 4985–4991. [CrossRef]
- 29. Zhang, M.; Ji, S.; Hu, L.; Yin, F.; Li, C.; Liu, H. Structural Characterization of Highly Stable Ni/SBA-15 Catalyst and Its Catalytic Performance for Methane Reforming with CO₂. *Chinese J. Catal.* **2006**, *27*, 777–781. [CrossRef]
- 30. Zhang, F.; Yan, Y.; Yang, H.; Meng, Y.; Yu, C.; Tu, B.; Zhao, D. Understanding Effect of Wall Structure on the Hydrothermal Stability of Mesostructured Silica SBA-15. *J. Phys. Chem. B* **2005**, *109*, 8723–8732. [CrossRef]
- 31. Kim, K.S.; Davis, R.E. Electron spectroscopy of the nickel-oxygen system. *J. Electron Spectrosc. Relat. Phenom.* **1972**, *1*, 251–258. [CrossRef]
- 32. Liu, X.; Khinast, J.G.; Glasser, B.J. A parametric investigation of impregnation and drying of supported catalysts. *Chem. Eng. Sci.* **2008**, *63*, 4517–4530. [CrossRef]
- 33. Munnik, P.; de Jongh, P.E.; de Jong, K.P. Recent Developments in the Synthesis of Supported Catalysts. *Chem. Rev.* **2015**, *115*, 6687–6718. [CrossRef] [PubMed]
- 34. Olea, M.; Hodgson, S.; Sasaki, T.; Aoki, N.; Mae, K. tap (temporal analysis of products) studies of the catalytic conversion of biogas to syngas over NI/SIO₂ catalysts. *Chem. Eng. Trans.* **2009**, *17*, 7–12.
- 35. Setiabudia, H.D.; Lima, K.H.; Ainirazalia, N.; China, S.Y.; Kamarudin, N.H.N. CO₂ reforming of CH₄ over Ni/SBA-15: Influence of Ni loading on the metal support interaction and catalytic activity. *JMES* **2017**, *8*, 573–581.
- 36. Liu, D.; Quek, X.-Y.; Wah, H.H.A.; Zeng, G.; Li, Y.; Yang, Y. Carbon dioxide reforming of methane over nickel-grafted SBA-15 and MCM-41 catalysts. *Catal. Today* **2009**, *148*, 243–250. [CrossRef]
- 37. Gerhartz, W. (Ed.) *Ullmann's Encyclopedia of Industrial Chemistry*, 5th ed.; VCH Publishers: Deerfield Beach, FL, USA, 1991; Volume A1, p. VA17.
- 38. Available online: http://www.engineeringtoolbox.com/surface-tension-d_962.html (accessed on 23 July 2025).
- 39. Qian, L.; Yan, Z. Mechanistic Study of Carbon Dioxide Reforming with Methane over Supported Nickel Catalysts. *J. Natural Gas Chem.* **2002**, *11*, 151–158.

Processes 2025, 13, 3505 22 of 22

40. Liu, D.; Lau, R.; Borgna, A.; Yang, Y. Carbon dioxide reforming of methane to synthesis gas over Ni-MCM-41 catalysts. *Appl. Catal. A Gen.* **2008**, *358*, 110–118. [CrossRef]

- 41. García-Dieguéz, M.; Pieta, I.S.; Herrera, M.C.; Larrubia, M.A.; Malpartida, I.; Alemany, L.J. Transient study of the dry reforming of methane over Pt supported on different *γ*-Al₂O₃. *Catal. Today* **2010**, *149*, 380–387. [CrossRef]
- 42. Suh, D.J.; Park, T.-J.; Kim, J.-H.; Kim, K.-L. Nickel–alumina aerogel catalysts prepared by fast sol–gel synthesis. *J. Non-Cryst. Solids* **1998**, 225, 168–172. [CrossRef]
- 43. Ahmed, R.; Sasaki, T.; Olea, M. Original method to predict and monitor carbon deposition on Ni-based catalysts during dry reforming of methane. *Front. Chem. Eng.* **2020**, *2*, 9. [CrossRef]
- 44. Ahmed, R. High-Efficiency Catalysts for Dry Reforming of Methane. Ph.D. Thesis, Teesside University, Middlesbrough, UK, 2013.
- 45. Iro, E.; Hajimirzaee, S.; Sasaki, T.; Olea, M. Novel Ni/SBA-15 catalyst pellets for tar catalytic cracking in a dried sewage sludge pyrolysis pilot plant. *Catalysts* **2025**, *15*, 142. [CrossRef]

Disclaimer/Publisher's Note: The statements, opinions and data contained in all publications are solely those of the individual author(s) and contributor(s) and not of MDPI and/or the editor(s). MDPI and/or the editor(s) disclaim responsibility for any injury to people or property resulting from any ideas, methods, instructions or products referred to in the content.